Chapter 3
Launching of Active Galactic Nuclei Jets

Alexander Tchekhovskoy

Abstract As black holes accrete gas, they often produce relativistic, collimated outflows, or jets. Jets are expected to form in the vicinity of a black hole, making them powerful probes of strong-field gravity. However, how jet properties (e.g., jet power) connect to those of the accretion flow (e.g., mass accretion rate) and the black hole (e.g., black hole spin) remains an area of active research. This is because what determines a crucial parameter that controls jet properties—the strength of large-scale magnetic flux threading the black hole—remains largely unknown. First-principles computer simulations show that due to this, even if black hole spin and mass accretion rate are held constant, the simulated jet powers span a wide range, with no clear winner. This limits our ability to use jets as a quantitative diagnostic tool of accreting black holes. Recent advances in computer simulations demonstrated that accretion disks can accumulate large-scale magnetic flux on the black hole, until the magnetic flux becomes so strong that it obstructs gas infall and leads to a magnetically-arrested disk (MAD). Recent evidence suggests that central black holes in jetted active galactic nuclei and tidal disruptions are surrounded by MADs. Since in MADs both the black hole magnetic flux and the jet power are at their maximum, well-defined values, this opens up a new vista in the measurements of black hole masses and spins and quantitative tests of accretion and jet theory.

3.1 Introduction

Black holes (BHs) of all sizes produce relativistic jets, one of the most spectacular manifestations of BH accretion. Figure 3.1 illustrates that jet-producing accretion systems span nearly 10 orders of magnitude in BH mass: from stellar-mass BHs in BH binaries (BHBs, Fig. 3.1c) and gamma-ray bursts (GRBs, Fig. 3.1d, e), with masses $M_{BH} \sim$ few $\times M_{\odot}$, to supermassive BHs in active galactic nuclei (AGN, Fig. 3.1a), with masses $M_{BH} \sim 10^{6-10} M_{\odot}$, where $M_{\odot} \approx 2 \times 10^{33}$ g is a solar mass. If a single mechanism is at work across the entire BH mass scale, it should be scale

A. Tchekhovskoy (✉)
Lawrence Berkeley National Laboratory, 1 Cyclotron Rd, Berkeley, CA 94720, USA
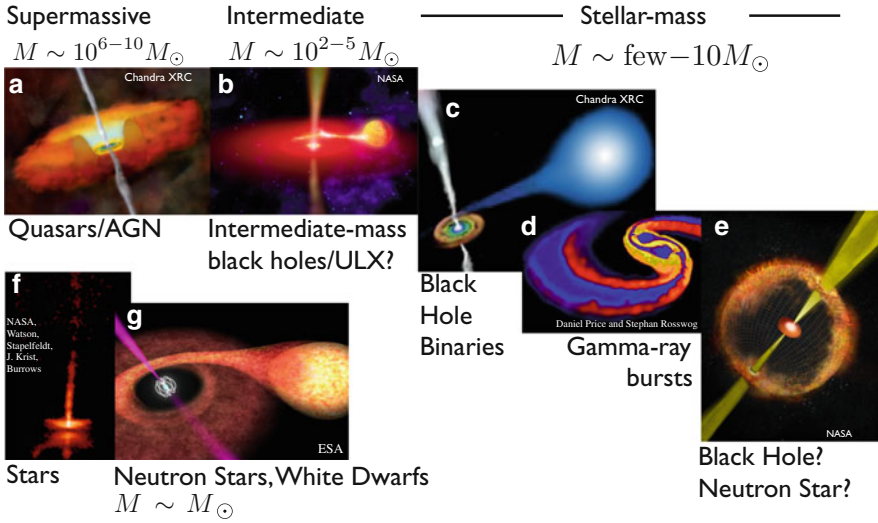e-mail: atchekho@berkeley.edu

Fig. 3.1 Black holes of all sizes produce jets. BHs come in two broad categories: supermassive, with masses ranging between millions and billions of solar masses, and stellar-mass BHs, with masses ranging from a few to tens of solar masses. Supermassive BHs are found at the centers of AGN (panel (**a**)), and stellar-mass BHs are found in binary systems (panel (**c**)), or formed as a result of binary neutron star mergers (panel (**d**)) and core collapse of massive stars that is thought to give rise to GRBs (panel (**e**)). Recent evidence suggests there is a third class of *intermediate-mass* BHs with masses bridging the mass gap (Hui and Krolik 2008; Farrell et al. 2009; Davis et al. 2011; Webb et al. 2012; Straub et al. 2014). To be fair to non-BH systems, the presence of an event horizon is not a necessity for producing jets: neutron stars (panels (**e**) and (**g**)) and white dwarfs (panel (**g**)), as well as normal stars (panel (**f**)), also produce jets

invariant. Magnetic fields are a promising agent for jet production because they are abundant in astrophysical plasmas and because the properties of magnetically-powered jets scale trivially with BH mass (Blandford and Znajek 1977; Chiueh et al. 1991; Heinz and Sunyaev 2003; Tchekhovskoy et al. 2008, 2009, 2010).

How are jets magnetically launched? Figure 3.2 shows a cartoon depiction of this. Consider a vertical magnetic field line attached on one end to a perfectly conducting sphere, which represents the central compact object, and on the other end to a perfectly conducting "ceiling", which represents the ambient medium (panel a). As the sphere is spinning at an angular frequency Ω, after N turns the initially vertical field line develops N toroidal field loops (panel b; we assume the ceiling is a distance $z_{\text{ceil}} \ll c/\Omega$ away from the central object, an assumption we later relax). This magnetic spring pushes against the ceiling due to the pressure of the toroidal field. As more toroidal loops form and the toroidal field becomes stronger, the spring pushes away the ceiling and accelerates any plasma attached to it along the rotation axis, forming a jet (panels (c) and (d) in Fig. 3.2, see the caption for details; after the ceiling is pushed away, the final state is independent of z_{ceil}). In the case when the central body is a BH, which does not have a surface, the rotation of space-time

a   **b**   **c**   **d**

$$p_{\mathrm{m}} = B_{\varphi}^2/8\pi$$

$$B_{\varphi} \gg B_z$$

$$v_{\mathrm{fluid}} \approx v_{\mathrm{field}}$$

field line

Ω

Ω

Φ

t=0   t=t$_1$ t=t$_2$ t=t$_2$
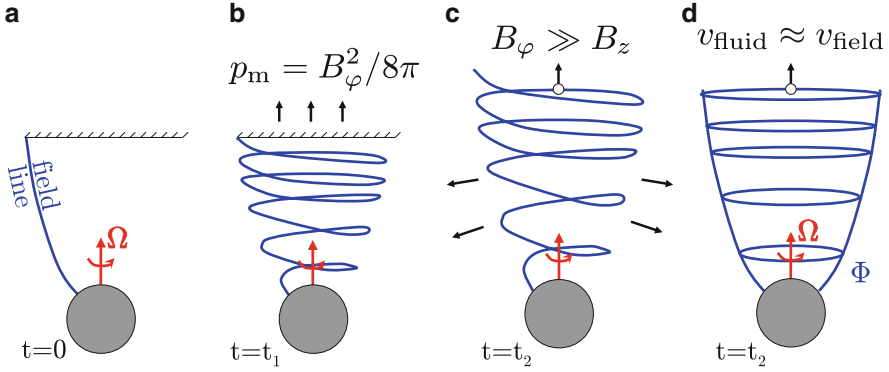
Fig. 3.2 Illustration of jet formation by magnetic fields. Panel (**a**): Consider a purely poloidal (i.e., toroidal field vanishes, $B_{\varphi} = 0$) field line attached on one end to a stationary "ceiling" (which represents the ambient medium and is shown with *hashed horizontal line*) and on the other end to a perfectly conducting sphere (which represents the central BH or neutron star and is shown with *gray filled circle*) rotating at an angular frequency Ω. Panel (**b**): After N rotations, at time $t = t_1$, the initially purely poloidal field line develops N toroidal loops. This magnetic spring pushes against the "ceiling" with an effective pressure $p_m \sim B_{\varphi}^2/8\pi$ due to the toroidal field, B_{φ}. As time goes on, more toroidal loops form, and the toroidal field becomes stronger. Panel (**c**): At some later time, $t = t_2$, the pressure becomes so large that the magnetic spring, which was twisted by the rotation of the sphere, pushes away the "ceiling" and accelerates the plasma attached to it along the rotation axis, forming a jet. Asymptotically far from the center, the toroidal field is the dominant field component and determines the dynamics of the jet. Panel (**d**): It is convenient to think of the jet as a collection of toroidal field loops that slide down the poloidal field lines and accelerate along the jet under the action of their own pressure gradient and tension (hoop stress). The rotation of the sphere continuously twists the poloidal field into new toroidal loops at a rate that, in steady state, balances the rate at which the loops move downstream. As we will see below (Sects. 3.3–3.4), the power of the jet is determined by two parameters: the rotational frequency of the central object, Ω, and the radial magnetic flux threading the object, Φ

causes the rotation of the field lines, and jets form in a similar fashion via a process referred to as Blandford-Znajek mechanism (BZ, hereafter) (Blandford and Znajek 1977).

3.2   Physical Description of Highly Magnetized Plasmas

To describe the motion of magnetized plasma on a curved space-time of a BH from first-principles is a formidable task. The relativistic analog of second Newton's law "$\mathbf{F} = m\mathbf{a}$" in the absence of gravity takes the form:

$$\rho_c \mathbf{E} + \mathbf{j} \times \mathbf{B} = \rho \frac{\mathrm{d}(\gamma \mathbf{v})}{\mathrm{d}t}, \tag{3.1}$$

where all quantities are measured in the lab frame: ρ is mass density and ρ_c is electric charge density, $\mathbf{E}$ and $\mathbf{B}$ are electric and magnetic field strengths, $\mathbf{j}$ is the electric current density, and γ and $\mathbf{v}$ are the Lorentz factor and velocity of the plasma. To close the system, we complement Eq. (3.1) with Maxwell's equations, $\nabla \cdot \mathbf{E} = 4\pi\rho_c$, $\partial\mathbf{E}/\partial t = c\nabla \times \mathbf{B} - 4\pi\mathbf{j}$, and $\partial\mathbf{B}/\partial t = -c\nabla \times \mathbf{E}$. For simplicity, in Eq. (3.1) we dropped non-magnetic forces (e.g., the thermal pressure term) on the left hand side.

In order to make progress, simplifications are necessary. The first simplification that is usually made is the assumption that the fluid is *ideal*, or infinitely conducting. That is, in the fluid frame the Ohm's law takes the form: $\mathbf{j}' = \sigma\mathbf{E}'$ with $\sigma = \infty$, where the prime symbols indicate quantities measured in the fluid frame. Since $\mathbf{j}'$ is finite, the electric field in the frame of the fluid vanishes: $\mathbf{E}' \propto \mathbf{E} + \mathbf{v} \times \mathbf{B}/c = 0$. This gives us the *ideal magnetohydrodynamics* (ideal MHD) approximation.

For highly magnetized plasmas even further simplification is possible. A particularly useful approach is to utilize a *force-free* approximation. It works well for the cases when magnetic field is so strong that the effects of inertia of plasma particles attached to the field lines as well as of pressure forces are negligible. This amounts to neglecting the right-hand side in Eq. (3.1). The resulting equation states that the left-hand side of Eq. (3.1), the force, vanishes. Hence, the name: *force-free* approximation.

Due to space constraints we will not be able to describe the details of ideal MHD and force-free approaches. We will only mention that both approaches can be generalized to a curved space-time of a spinning BH, and the resulting sets of equations can be solved either analytically or numerically, with examples of such solutions given below.

3.3   Extraction of BH Rotational Energy via Magnetic Field

Magnetic Field Configuration Consider a rotating BH threaded with a force-free magnetic field. The simplest magnetic field configuration of this type is a BH with a nonzero magnetic monopole charge, as illustrated in Fig. 3.3a. While such a configuration may seem unrealistic—after all, magnetic monopoles do not exist!—this not quite so. Energetically, this is equivalent to a *split-monopole* configuration, in which magnetic field direction reverses in the equatorial plane, as shown in Fig. 3.3b. The split-monopole has no monopole charge on the BH: the magnetic field is sourced by an equatorial current sheet. The modern thinking is that the current sheet represents the current carried by the plasma in a razor-thin accretion disk orbiting the BH (Blandford and Znajek 1977). As we will see below, this is indeed a good description of reality (see Fig. 3.9b). An even more realistic field configuration is a parabolic one, illustrated in Fig. 3.3c: it also has an equatorial current sheet, but now the field lines thread not only the BH but also the sheet. This configuration is qualitatively similar to what is found in numerical BH accretion-jet simulations, as we will see below (see, e.g., Fig. 3.9b).
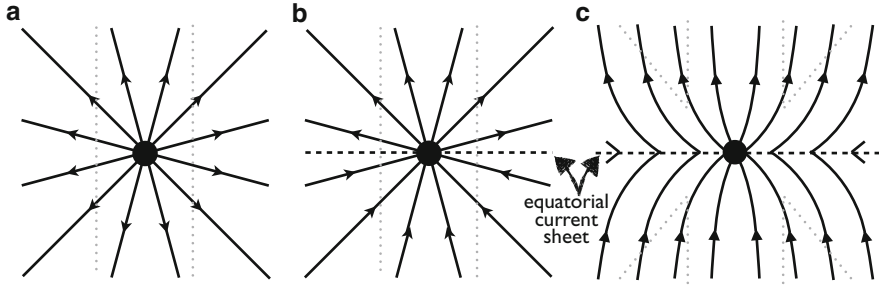
Fig. 3.3 Magnetic field configurations around a BH. First, consider a non-rotating BH. Panel (**a**) shows a BH, indicated with the *black filled circle*, threaded with *monopolar* (radial) magnetic field B_r. This is the simplest configuration for computing BH power output. Since it implies the presence of a nonzero magnetic (monopole) charge on the hole, by analogy with the electric charge, this configuration is a solution to force-free equations. Whereas it might seem that this solution is artificial (because magnetic monopoles do not exist), with a small modification we can convert it to a physical solution. Panel (**b**) shows a BH with a *split-monopolar* magnetic field. In this configuration, the magnetic field is also radial but changes direction across the equatorial plane. Unlike panel (**a**), here the radial magnetic field is monopole-free and is sourced by an equatorial current sheet, which is shown with the *black dashed line*. The modern thinking is that the current sheet represents the current carried by the plasma in a razor-thin accretion disk orbiting the BH (Blandford and Znajek 1977). (As we will see below, in jet-producing BHs, accretion disks are thought to be geometrically-thick (Sect. 3.5), therefore their current is a distributed current rather than a singular current (see Fig. 3.9b).) Due to the equatorial symmetry, the magnetic fields are in force-balance across the current sheet; therefore, just like the configuration in panel (**a**), what we have here is also a solution to force-free equations. Now suppose the BH is spinning. Due to rotation, each field line winds up, develops an azimuthal field component B_φ (not shown here) and rotates at an angular frequency Ω_F (which can vary from one field line to another but is a constant along each of the field lines). The rotation brings about a characteristic length scale, $R_{LC} = c/\Omega_F$, that is indicated by *gray vertical dotted lines* and is called the *light cylinder* (LC, Eq. 3.4). Panel (**c**) shows a BH with a parabolic magnetic field. This configuration is more realistic than the ones in panels (**a**) and (**b**): it is closer to what is found in global numerical simulations of accreting BHs (as we will later; see, e.g., Fig. 3.9b). In this configuration the field lines thread not only the BH but also the current sheet. The field lines threading the sheet can be thought of as being powered by the rotation of the razor-thin disk, which is represented by the current sheet. Since angular frequency Ω_F differs from one field line to another in this configuration (e.g., disk field lines can rotate slower than BH field lines), the LC does not have a cylindrical shape

Black Hole "Hairs" A *nonrotating* BH is charaterized by two "hairs": mass M_{BH} and charge Q_{BH}. The charge of astrophysical BHs is thought to be negligibly small to affect the gravity of the BH,[1] thus we will set $Q_{BH} = 0$ for the rest of our discussion. In addition to M_{BH}, an astrophysical *rotating* BH is characterized by the value of its angular momentum J_{BH}, or, equivalently, dimensionless BH spin, $a = J_{BH}/J_{max}$. Here $r_g = GM_{BH}/c^2$ is BH gravitational radius, $J_{max} = M_{BH}r_g c$ is the maximum angular momentum a BH of mass M_{BH} can have, and c is the speed

---

[1]If a BH were strongly charged, it would attract oppositely-charged particles, which would neutralize the BH charge.

of light. Thus defined, BH spin varies from 0 (nonspinning BHs) to 1 (maximally spinning BHs).

Rotation of Black Hole and Magnetospheric Structure BH rotation causes the inertial frames to be dragged about the BH at an angular frequency, $\Omega \approx \Omega_H \times (r/r_H)^{-3}$, where

$$\Omega_H = \frac{ac}{2r_H} \tag{3.2}$$

and $r_H = r_g(1 + \sqrt{1-a^2})$ are the angular frequency and radius of BH event horizon, respectively. For convenience we will also use a normalized version of Ω_H:

$$\omega_H \equiv \frac{\Omega_H}{\Omega_{H,max}} \equiv \frac{2r_g\Omega_H}{c} \equiv \frac{a}{1 + \sqrt{1-a^2}}. \tag{3.3}$$

Frame-dragging attempts to force different parts of the field line to rotate at different frequencies: $\Omega = \Omega_H$ near the BH and $\Omega = 0$ at infinity. However, in a steady state every field line must rotate at a single angular frequency.[2] Understandably, this forces a field line to choose an in-between value of Ω, which turns out to be close to the average of the two frequencies, $\Omega_F \simeq 0.5\Omega_H$ (Blandford and Znajek 1977; Tchekhovskoy et al. 2010).

The rotational frequency introduces a characteristic length scale into the problem,

$$R_{LC} = \frac{c}{\Omega_F}, \tag{3.4}$$

which is referred to as the *light cylinder* (LC) radius. It has a clear physical meaning: if a magnetic field line rigidly rotates at an angular frequency Ω_F, its rotational velocity reaches the speed of light at a cylindrical radius R_{LC}. At the LC, special relativistic effects become important, and all components of electromagnetic field become comparable: $B_\varphi \sim E_\theta \sim B_r \sim \Phi_{BH}/2\pi R_{LC}^2$, where Φ_{BH} is the magnetic flux through the BH, B_r and B_φ are radial and toroidal magnetic field components, and E_θ is the θ-component of electric field. Note that the LC is of cylindrical shape only if $\Omega_F = $ const; if this is not the case, as illustrated in Fig. 3.3c, the shape of the LC can be very different from a cylinder. Yet, it is often referred to by the same name—"light cylinder"—regardless of this.

---

[2]If this were not the case, differential rotation between different parts of the field line would cause the production of new toroidal magnetic field loops and the violation of steady-state assumption, similar to the process illustrated in Fig. 3.2a, b.

3.4 BH Spindown Power

We can approximately compute the spindown power of a BH as the product of characteristic values of the Poynting flux and the area of the LC:

$$P \sim \frac{c}{4\pi}\,(\mathbf{E} \times \mathbf{B})_r \times 4\pi R_{LC}^2 = cE_\theta B_\varphi R_{LC}^2 \sim \frac{1}{16\pi^2 c}\Phi_{BH}^2 \Omega_H^2 = \frac{c}{64\pi^2 r_g^2}\Phi_{BH}^2\omega_H^2,$$

(3.5)

where we used the fact that $\Omega_F \approx 0.5\Omega_H$ and that at the LC one has $E_\theta \sim B_\varphi \sim \Phi_{BH}/2\pi R_{LC}^2$. This estimate is within a factor of 2 of a more detailed calculation that gives the 2nd-order accurate expansion of spindown power in powers of ω_H (Tchekhovskoy et al. 2010),

$$P_{BZ2} = \frac{c}{96\pi^2 r_g^2}\Phi_{BH}^2\omega_H^2. \qquad \text{(2nd order BZ2 expansion, } a \lesssim 0.95)$$

(3.6)

For rapidly rotating BHs, magnetic field lines tend to bunch up toward the rotational axis, which leads to higher order corrections in the expression for jet power relative to the 2nd order expansion (3.6). These corrections are captured by the 6th order accurate expansion (Tchekhovskoy et al. 2010):

$$P_{BZ6} = \frac{\kappa c}{16\pi r_g^2}\Phi_{BH}^2\omega_H^2 \times f(\omega_H), \qquad \text{(6th order BZ6 expansion, all } a)$$

(3.7)

where factor

$$f(\omega_H) = 1 + 0.35\omega_H^2 - 0.58\omega_H^4$$

(3.8)

is a high-spin correction. Here prefactor κ weakly depends on magnetic field geometry, varying from $\kappa \approx 0.045$ for collimating, parabolic magnetic field geometry to $\kappa = 1/6\pi \approx 0.053$ for (split-)monopolar geometry (Tchekhovskoy et al. 2010). Figure 3.4 shows that the second-order BZ2 formula remains accurate for $a \lesssim 0.95$, but over-predicts the power by about 30 % as $a \to 1$.

These results are qualitatively similar to the findings of the pioneering Blandford-Znajek (BZ) work (Blandford and Znajek 1977), but there is difference on a quantitative level. BZ performed an expansion of BH energy loss rate in powers of a, not ω_H, and wrote down the following scaling:

$$P_{BZ} = \frac{\kappa c}{48\pi r_g^2}\Phi_{BH}^2 a^2 \qquad \text{(standard BZ expansion, low} - \text{spin limit, } a^2 \ll 1),$$

(3.9)

As is clear from Fig. 3.4, this low-spin approximation, which we refer to as the standard BZ formula, remains accurate up to $a \lesssim 0.5$ (Komissarov 2001; Tanabe and Nagataki 2008) and for high spin under-predicts the energy loss rate by a factor
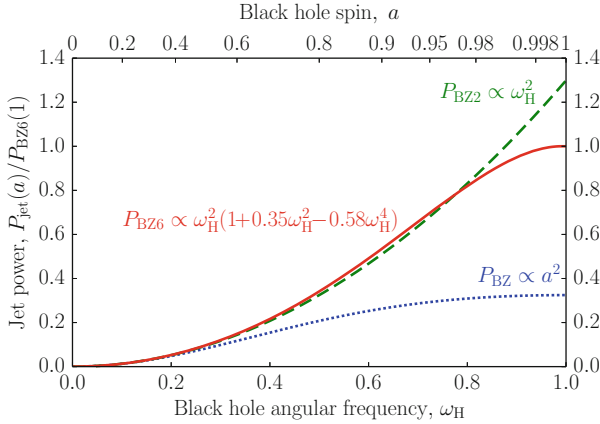
Fig. 3.4 Comparison of various approximations for jet power, P_{jet}, versus BH dimensionless angular frequency, ω_H (lower x-axis), and BH spin, a (upper x-axis). All powers are normalized to the maximum achievable power in the BZ6 approximation (Eq. 3.7), $P_{jet} \propto \omega_H^2(1 + 0.35\omega_H^2 - 0.58\omega_H^4)$, which is shown with *solid red line* and which remains accurate for all values of BH spin (Tchekhovskoy et al. 2010). A simpler BZ2 approximation (Eq. 3.6), $P_{jet} \propto \omega_H^2$, shown with *green dashed line*, is accurate up to $a \lesssim 0.95$, beyond which it over-predicts the power by about 30%. The standard BZ approximation (Eq. 3.9; Blandford and Znajek 1977), $P_{jet} \propto a^2$, shown with *blue dotted line*, remains accurate only for moderate values of spin, $a \lesssim 0.5$, beyond which it under-predicts the true jet power by a factor of ≈ 3

of 3. Therefore, when quantitative understanding of BH jet power is required, it is advantageous to use Eq. (3.6) (for $a \lesssim 0.95$) or Eq. (3.7) (for all values of spin).

3.5 When Are Jets Launched by Accreting Black Holes?

The factors that control whether a BH produces jets are not well-understood. Observationally, it is clear that jet production is intimately related to the *spectral state* of the accretion disk (Fender et al. 2004). In Fig. 3.5, we identify 3 such states (see Remillard and McClintock 2006 for a detailed review). We classify them by their normalized luminosity, or the Eddington ratio, $\lambda = L/L_{Edd}$, where L is accretion luminosity and $L_{Edd} \approx 1.2 \times 10^{38} M_{BH}/M_\odot$ (erg s^{-1}) is the Eddington luminosity at which the outward radiation force on the electrons balances the inward gravitational force on the ions (see e.g. Frank et al. 2002).

Spectral States of BH Accretion: Thin-disk State We will start our discussion with the simplest and best understood state of accretion: the standard, geometrically-thin disk state, which is also referred to as "high/soft" state or "thermal" state (Shakura and Sunyaev 1973; Novikov and Thorne 1973); for a detailed description of these states and their properties with an emphasis on the accretion flow structure and emission, see Begelman (1985). This state, illustrated in Fig. 3.5b, occurs
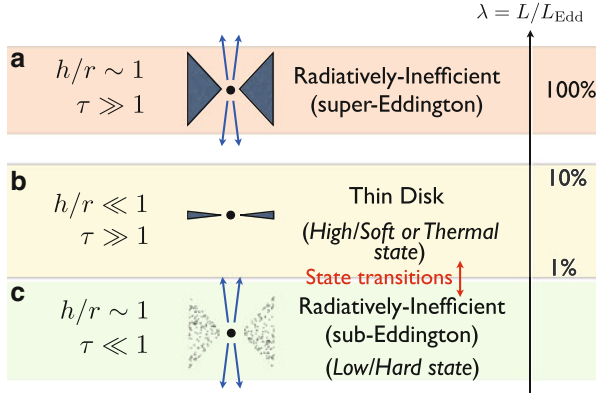
Fig. 3.5 Simplified picture of spectral states of BH accretion. The states are ordered by the value of dimensionless luminosity: the Eddington ratio, $\lambda = L/L_{\rm Edd}$. The BH is shown with a *black circle*, and the accretion disk with a *dark blue wedge*. The presence of jets is indicated with *blue arrows*. For convenience of presentation, we start with panel (**b**), move on to (**c**), and then to (**a**). Panel (**b**): The "thin disk" state—or as it is also referred to, "high/soft" or "thermal" state— occurs between $\sim 1\%$ and few $\times 10\%$ of $L_{\rm Edd}$ and is the best understood state of all accretion spectral states. Disk gas rotates on Keplerian orbits. Viscosity causes it to gradually lose its angular momentum and very slowly march inward, moving from one Keplerian orbit to another. The gas is optically-thick, $\tau \gg 1$, which means that it radiates as a blackbody. In fact, it takes much longer for the gas to reach the BH than to radiate viscously generated energy, so all viscously generated energy is radiated as the location where it was produced, i.e., the disk is *radiatively-efficient*. This keeps the disk cool and geometrically-thin, $h/r \ll 1$. Panel (**c**): Let us imagine that we start with the "thin disk" state and decrease $\dot{M}$ such that $L \lesssim 0.01 L_{\rm Edd}$. The disk enters the "low/hard" state: disk density drops, and the inner disk becomes optically thin, $\tau \ll 1$, which is illustrated in the figure by the light shading of the disk wedge. This makes it difficult for the disk to cool. Now, the viscously-generated energy, instead of being radiated right away, is locked into the accretion flow, with most of the energy ending up in the BH and only a small fraction escaping as radiation, i.e., the disk is *radiatively-inefficient*. This causes the disk to get hotter and puff up, leading to $h/r \sim 1$. Panel (**a**): Now let us imagine that we start with the "thin disk" state and increase $\dot{M}$ well above Eddington, such that $L \gtrsim L_{\rm Edd}$. In order to accommodate the increased mass supply, disk density, thickness, and radial velocity increase. Disk rotation becomes sub-Keplerian. Due to the higher disk density and thickness, the disk becomes optically-thick, $\tau \gg 1$, and the time it takes for photons to diffuse out of the disk body increases and becomes longer than the time it takes for the gas to reach the BH. This means that most of the photons are locked up inside the accretion flow and end up in the BH, with only a small fraction escaping, i.e., the disk is *radiatively-inefficient*. **Jet launching and spectral state transitions**: Spectral states with geometrically-thick disks, like in panels (**a**) and (**c**), produce jets (indicated with *blue arrows*), whereas geometrically-thin disks do not. In addition to continuous jets discussed above, transient jets can be produced during "hard" to "soft" disk spectral *state transitions* (state c→b). See text for details

between about one and a few tens of per cent of Eddington, or roughly $L \sim (0.01-1)L_{\rm Edd}$ (see e.g. Maccarone 2003). Disk gas rotates on Keplerian orbits. Viscosity causes it to gradually lose its angular momentum and very slowly march inward, moving from one Keplerian orbit to another. The source of viscosity is most likely the magnetorotational instability (MRI, Balbus and Hawley 1991),

which amplifies any weak magnetic field in the accretion disk to sub-equipartition levels and transports angular momentum outward and gas inward. The gas is optically-thick, with optical depth $\tau \gg 1$, which means that parcels of gas on different Keplerian orbits radiate as blackbodies at their own temperatures (hence the name "thermal" state). The integrated spectrum is often referred to as "multicolor blackbody" spectrum. Due to the low radial velocity, it takes much longer for the gas to reach the BH than to radiate viscously generated energy, so all viscously generated energy is radiated *locally*, at the location where it is produced, i.e., the disk is *radiatively-efficient*. This keeps the disk cool and geometrically-thin, $h/r \ll 1$. The radiative efficiency of the disk, defined as $\epsilon = L/\dot{M}c^2$, is between 0.05 for non-spinning BHs and $\simeq 0.3$ for nearly maximally-spinning BHs (Novikov and Thorne 1973) (see also Shapiro and Teukolsky 1986; Frank et al. 2002). In many observational applications, authors often set disk radiative efficiency to a characteristic value $\epsilon_d = 0.1$ and define Eddington mass accretion rate $\dot{M}_{Edd} = L_{Edd}/\epsilon_d c^2 = 10 L_{Edd}/c^2$.

Sub-Eddington Thick-disk State Let us imagine that we start with the "thin disk" state and decrease $\dot{M}$ such that $L \lesssim 0.01 L_{Edd}$. The disk enters the "low/hard" state illustrated in Fig. 3.5c: disk density drops, and the inner disk becomes optically thin, $\tau \ll 1$ (Esin et al. 1997, 1998). This makes it difficult for the disk to cool. Now, the viscously-generated energy, instead of being radiated right away, is locked into the accretion flow, with most of the energy ending up in the BH and only a small fraction escaping as radiation, i.e., the disk is *radiatively-inefficient*. This causes the disk to get hotter and puff up, causing it to become geometrically-thick, $h/r \sim 1$. See Yuan and Narayan (2014) for a recent review of radiatively-inefficient sub-Eddington accretion.

Super-Eddington Thick-disk State Now let us imagine that we start with the "thin disk" state and increase $\dot{M}$ well above $\dot{M}_{Edd}$, such that $L \gtrsim L_{Edd}$, as illustrated in Fig. 3.5a. In order to accommodate the increased mass supply, disk density, thickness, and radial velocity increase. Disk rotation becomes sub-Keplerian. Due to the higher disk density and thickness, the disk becomes optically-thick, $\tau \gg 1$, and the time it takes for photons to diffuse out of the disk body increases and becomes longer than the time it takes for the gas to reach the BH. This means that most of the photons are locked up inside the accretion flow and end up in the BH, with only a small fraction escaping, i.e., the disk is *radiatively-inefficient*. Note that whereas mass accretion rate can exceed Eddington by essentially any factor (i.e., $\dot{M} \ggg \dot{M}_{Edd}$ is possible), the emerging radiation is always limited by a logarithmic factor times the Eddington luminosity limit, i.e., $L \lesssim$ few $\times L_{Edd}$. At the same time, the emission can be beamed into a small solid angle, so an observer exposed to it assuming that the emission is isotropic will incorrectly conclude that the source is a highly super-Eddington emitter (Sądowski et al. 2014; McKinney et al. 2014). There are several observational examples of highly super-Eddington accretion. Gamma-ray bursts, which accrete at $\dot{M} \sim 0.1 M_\odot \text{s}^{-1}$, have $\dot{M}/\dot{M}_{Edd} \sim 10^{13} \ggg 1$. Recent evidence suggests that supermassive BHs can accrete at a respectable $\dot{M}/\dot{M}_{Edd} \sim 100 \gg 1$ (see Sect. 3.10).

Nature of Low Radiative Efficiency Perhaps somewhat surprisingly, both super-Eddington state in Fig. 3.5a and sub-Eddington state in Fig. 3.5c are radiatively-inefficient, but for very different reasons. The super-Eddington accretion flow is radiatively-inefficient because the disk is so optically-thick that it takes longer for a photon to diffuse out of the gas than for the gas fall into the hole. In contrast, the sub-Eddington accretion is radiatively inefficient because viscous dissipation predominantly heats the ions. Due to the low density, the ions do not talk to electrons, which are responsible for radiation. As a result, we end up with a *two-temperature* accretion flow, in which the heat is locked up with the ions, whereas the electrons, responsible for radiation, remain relatively cold (Begelman 1985; Yuan et al. 2003). In our simulations described below, we concentrate on sub- and super-Eddington radiatively-inefficient accretion, and we will neglect radiative cooling.

Jet Launching and Spectral State Transitions Spectral states with geometrically-thick disks, like in Fig. 3.5a, c, produce jets (indicated with blue arrows), as evidenced by observations of AGN and BHBs. Such jets are called *continuous* jets. In contrast, geometrically-thin disks, like in Fig. 3.5b, produce neither jets nor the associated radio emission (Fender et al. 2004; Russell et al. 2011), as seen in BHBs and many AGN. There are competing explanations as to why geometrically thin disks are jet phobic, but no clear winner. As discussed above, geometrically-thin disks have a low radial velocity. Thus, one can argue that magnetic fields diffuse outward faster than the accretion disk drags them inward (Lubow et al. 1994; Guilet and Ogilvie 2012, 2013), so there is no large-scale magnetic flux to power the jets (however, see Rothstein and Lovelace 2008). (This is not a problem for geometrically-thick disks, which have a large radial velocity.) Another possibility is that thin disks do not provide enough collimation to the emerging outflow, as opposed to thick disks. It is possible that not one single factor but a combination of several factors is responsible for the inability of geometrically-thin disks to produce jets.

In addition to continuous jets discussed above, *transient* jets are observed *during* disk spectral "hard to soft" state transitions and are indicated in Fig. 3.5b, c with the two-sided red arrow (see Fender et al. 2004 for more details). During such transitions, disk luminosity L spikes up from $\lesssim 0.01 L_{Edd}$ to $\sim L_{Edd}$. Disk spectrum becomes strongly distorted, presumably by the hot and highly magnetized "corona" that sandwiches the disk, and has little resemblance with the black-body–like spectrum of the standard geometrically-thin disk, until the luminosity drops down to $\sim 0.1 L_{Edd}$. Such outbursts lead to jets that appear as discrete radio-emitting blobs of plasma ejected from the central BH. The power of transient jets is higher than that of continuous jets (Fender et al. 2004). Most of the observational evidence on state transitions comes from BHBs, or microquasars, for which state transitions occur over a period of days, but sometimes cycle over timescales of weeks or months. In AGN, or quasars, observing such state transitions is much harder, since the characteristic time scale, set by the mass of the central BHs, is $\sim 10^7-10^8$ times longer (for BH mass of $10^8-10^9 M_\odot$) than in BHBs. Thus, if the duration of state transitions scales by the same factor, it is of order of 10^4-10^7 years. Consequently, in any given AGN, we have no chance of observing a state transition from start to finish.

It is presently unclear what causes the production of continuous and transient jets, and there is no agreement on whether they share the same production mechanism. The simplest possibility is that both types of jets are produced by the same BZ-type process (Sect. 3.3) involving the extraction of BH rotational energy, and the differences in their power and timing properties are due to the differences in the supply of BH magnetic flux, Φ_{BH}, that powers the jets. Other suggestions include large-scale magnetic reconnection as the cause of transient jets (Igumenshchev 2009; Dexter et al. 2014). A separate question is what causes the rise in the accretion rate during the state transition, and the answer is presently unclear. It is plausibly related to a global instability of the accretion flow that gives rise to an increased angular momentum transport; such an instability could be driven by temperature-sensitive turbulent transport in the disk (Potter and Balbus 2014) or the accumulation of large-scale magnetic flux (Begelman and Armitage 2014). We will return to the question of state transitions in Sects. 3.7 and 3.8.

3.6 What Sets Jet Power of Accreting Black Holes?

We have shown that BH power is directly proportional to the square of BH magnetic flux, Φ_{BH}, and the square of BH angular frequency, Ω_H (see Eq. 3.7), with small corrections beyond $a \gtrsim 0.95$. In nature, Φ_{BH} is a free parameter, whose value is poorly observationally constrained. Based on dimensional analysis, we have $\Phi_{BH} \propto \dot{M}^{1/2}$. But what sets the dimensionless ratio,

$$\phi_{BH} = \frac{\Phi_{BH}}{(\langle \dot{M} \rangle r_g^2 c)^{1/2}}, \tag{3.10}$$

which characterizes the degree of inner disk magnetization and controls energy extraction from the BH (Gammie et al. 1999; Komissarov and Barkov 2009; Penna et al. 2010; Tchekhovskoy et al. 2011; Tchekhovskoy and McKinney 2012; McKinney et al. 2012)? Here $\langle \ldots \rangle$ is a time-average. Using ϕ_{BH}, we define BZ efficiency as BZ6 power (Eq. 3.7) normalized by $\dot{M}c^2$:

$$\eta_{BZ} = \frac{P_{BZ}}{\langle \dot{M} \rangle c^2} \times 100\% = \frac{\kappa}{16\pi} \phi_{BH}^2 \omega_H^2 f(\omega_H) \times 100\%, \tag{3.11}$$

where $f(\omega_H)$ is a high-spin correction given in Eq. (3.8).

The physical meaning of η_{BZ} is simple: it is energy investment efficiency into the BH. Let us consider a practical example. Since mass is energy ($E = Mc^2$) and energy is money, suppose you have a hundred dollars (euros, yen, etc.; pick your favorite currency) worth of energy. And suppose you decide to invest it into a BH: you drop the 100 dollars worth of mass-energy into the BH and 20 comes back out. In this case the energy investment efficiency into the BH is $\eta_{BZ} = 20\%$. That seems quite low: you just lost 80 dollars! But suppose you get 150 dollars back: that

would be a much better outcome. In fact, you would get more out of the BH that you put in. Where would the extra 50 dollars worth of energy come from? It would come from the BH spin energy: BH rotation slows down and the released rotational energy powers the outflow. In a moment we will see how this occurs in a realistic astrophysical setting.

For the rest of the discussion we will make a distinction between (i) outflows powered by the rotation of the central BHs, which we will refer to as the "jets" and whose power we will denote as P_{jet} (which turns out to be very close to P_{BZ}), and (ii) outflows powered by the rotation of the accretion disks, which we will refer to as "winds" and whose power we will denote as P_{wind}. The sum of the two by definition gives the total outflow power, $P_{outflow} = P_{jet} + P_{wind}$, and the total outflow efficiency,

$$\eta = \frac{P_{outflow}}{\langle \dot{M} c^2 \rangle} \times 100\% \tag{3.12}$$

Until recently, general relativistic MHD simulations of jet formation found a rather low jet production efficiency: $\eta_{BZ} \lesssim 20\%$, even for nearly maximally spinning BHs (McKinney 2005; De Villiers et al. 2005; Hawley and Krolik 2006; Barkov and Baushev 2011). Moreover, the larger is the large-scale magnetic flux initially present around the BH, the stronger are the jets (McKinney and Gammie 2004; McKinney 2005; Beckwith et al. 2008; McKinney and Blandford 2009; McKinney et al. 2012). Thus, even for a fixed value of BH spin, variations in large-scale poloidal magnetic flux supply are expected to lead to variations in η_{BZ}: some systems would have no jets at all ($\eta_{BZ} = 0$), some systems would have very strong jets, and the rest would lie in between. A fundamental question emerges: do we expect there to be a limit on how powerful jets can be? If such a limit exists, what does it tell us about the physical processes responsible for jet production?

This is an especially important question since observations suggest high energy efficiency of outflow production (Rawlings and Saunders 1991; Fernandes et al. 2011; Ghisellini et al. 2010; Punsly 2011; McNamara et al. 2011), $\eta \gtrsim 100\%$. Can magnetic fields produce jets at such a high efficiency? If yes, then magnetic outflow models are viable. If not, a revision of the models is in order.

Suppose somebody gave us a BH, so its mass and spin are given, and we are interested in extracting its spin energy in the most efficient way possible. According to Eq. (3.6) (or its more accurate version, Eq. (3.7)), to maximize BH power, we need to maximize BH magnetic flux, Φ_{BH}. But what sets the maximum value of Φ_{BH}? To answer this fundamental question, consider a BH immersed into a vertical magnetic field at the center of an accretion disk, as shown in Fig. 3.6. The magnetic pressure force, which can be estimated as magnetic pressure times characteristic surface area, $F_B \sim (B^2/8\pi) \times 4\pi r^2 \times (h/r)$, pushes outward on the accretion disk. Clearly, if we removed the disk, the magnetic field would leave the BH due to the "no-hair theorem", which states that an isolated BH can only possess mass, spin, and charge, but not magnetic field or magnetic flux (see Sect. 3.3). Thus, it is the weight of the disk, or the associated force of gravity, $F_G \sim GM_{BH}M_{Disk}/r^2$, that keeps the magnetic field from leaving the BH. The disk must be massive enough to keep the magnetic flux on the BH: $F_B < F_G$. If the opposite is true, i.e. if the magnetic
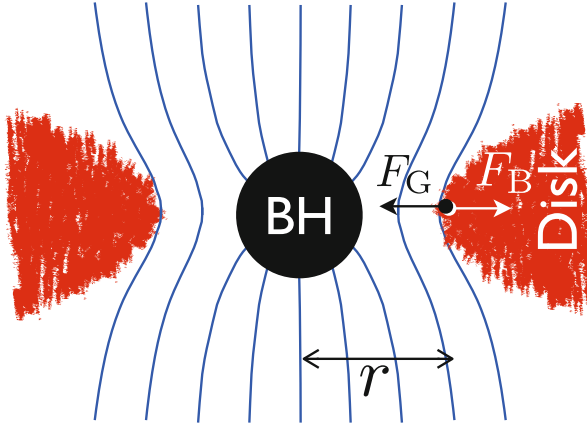
Fig. 3.6 Vertical slice through BH accretion system illustrates how the balance of forces determines the maximum possible field strength on the BH. The BH, shown as a *black circle*, is threaded with vertical magnetic field, whose lines of force are shown with *blue lines*. The magnetic pressure force, F_B, pushes outward on the accretion disk gas, which is shown in *red*. Clearly, if we removed the disk, the magnetic field would leave the BH due to the "no-hair theorem", which states that an isolated BH can only possess mass, spin, and charge, but not magnetic flux (Sect. 3.3). Thus, it is the weight of the disk, or the associated force F_G, that keeps the magnetic field from leaving the BH. The disk must be massive enough to keep the magnetic flux on the BH: $F_B < F_G$. If the opposite is true, i.e. if the magnetic field gets too strong, it pushes parts of the disk away, the excess magnetic field leaves, and the accretion flow enters a *magnetically-arrested disk* (MAD) state (Bisnovatyi-Kogan and Ruzmaikin 1974, 1976; Igumenshchev et al. 2003; Narayan et al. 2003; Igumenshchev 2008; Tchekhovskoy et al. 2011; Tchekhovskoy and McKinney 2012; McKinney et al. 2012). A characteristic size $r \sim$ few $\times r_g$ involved into the force balance is indicated

field gets too strong, it pushes parts of the disk away, and the excess magnetic field leaves. The accretion flow then becomes the *magnetically-arrested disk*, or a MAD (Bisnovatyi-Kogan and Ruzmaikin 1974, 1976; Igumenshchev et al. 2003; Narayan et al. 2003; Igumenshchev 2008; Tchekhovskoy et al. 2011; Tchekhovskoy and McKinney 2012; McKinney et al. 2012). In this state the magnetic field on the BH and the jet power are maximum, and we discuss this state in detail below.

Thus, the maximum possible magnetic field strength on the hole is given by the condition $F_B = F_G$. We write disk mass as $M_{Disk} \sim \rho \times (4\pi r^3/3) \times (h/r)$, and get:

$$\frac{B^2}{8\pi}4\pi r^2 = \frac{GM_{BH}\rho 4\pi r^3/3}{r^2}. \tag{3.13}$$

Now, using mass continuity equation $\dot{M} = 4\pi r^2 \rho v_r \times (h/r)$ to eliminate gas density ρ, where v_r is radial velocity of the infalling gas, we obtain an estimate of field strength at the BH event horizon:

$$B_{MAD} \sim 2 \times 10^4 \, [\text{G}] \left(\frac{L}{0.1 L_{Edd}}\right)^{1/2} \left(\frac{M_{BH}}{10^9 M_\odot}\right)^{-1/2} \left[\frac{(v_r/c) \times (h/r)}{0.05}\right]^{-1/2}, \tag{3.14}$$

where we took $r = r_H = 2r_g$ for a non-spinning BH. This magnetic field strength is quite reasonable for AGN (Begelman 1985), so it is possible that at least some AGN can reach the MAD limit. In terms of dimensionless magnetic flux, we obtain:

$$\phi_{MAD} \sim 30 \left[\frac{(v_r/c) \times (h/r)}{0.05} \right]^{-1/2}. \tag{3.15}$$

Here we adopted characteristic values: $v_r \sim c$, because gas falls into the BH at near the speed of light, and $h/r \sim 0.05$, because—as we will see below—strong BH magnetic field squeezes the disk vertically down to $h/r \sim 0.05$ near the BH from $h/r \sim 0.3-1$ at large distances. Estimate (3.15) is quite similar to what we will see in the numerical simulations.

MAD vs SANE Initial Conditions We tested the above non-relativistic consideration of force-balance near the BHs with global time-dependent general relativistic MHD accretion disk-jet simulations for different values of BH spin. As is standard, we initialized the simulation with a hydrodynamic gas torus on an orbit around a BH (Chakrabarti 1985; De Villiers and Hawley 2003a), as seen in Fig. 3.7a–d. The gas is in equilibrium under the action of the force of gravity pulling it inward, the centrifugal force pushing it outward, and the thermal pressure gradient balancing the difference between these two forces. That the torus is in equilibrium means that if left alone, it would orbit the BH indefinitely. In order for the gas to accrete, it is standard to insert into the torus a poloidal ($B_\varphi = 0$) magnetic field loop, which is shown in Fig. 3.7a–d with solid black lines. This magnetic field is unstable to the MRI (see Sect. 3.5 and Balbus and Hawley 1991), which drives the accretion of gas and magnetic field on to the BH. We choose a weak magnetic field, with the ratio of gas to magnetic pressures, $\beta = p_{gas}/p_{mag} \geq 100 \gg 1$, so as not to disturb torus' initial equilibrium state and allow the MRI to fully develop.

Clearly, jet efficiency (Eq. 3.11) depends on the amount of large-scale magnetic flux Φ_{BH}, and time-dependent numerical simulations show that the larger the large-scale vertical magnetic flux in the initial torus, the more efficient the jets (McKinney and Gammie 2004; McKinney 2005; Beckwith et al. 2008; McKinney and Blandford 2009; McKinney et al. 2012). To maximize jet efficiency, we would like to populate the torus with a much larger magnetic flux than in previous work. In fact, our goal is for the torus to contain more magnetic flux than the inner disk can push into the BH. For these reasons, we choose a rather large torus capable of holding an extended magnetic flux distribution: the torus extends from $r_{in} = 15r_g$ to $r_{out} = \text{few} \times 10^4 r_g$, with the torus density peaking at $r_{max} = 34r_g$ (Fig. 3.7a–d). We also choose a rapidly spinning BH, $a = 0.99$. The large size of the torus allows us to insert a large poloidal magnetic field loop into it, with its center, or the O-point (pronounced "oh point"), located at $r_O \simeq 600r_g$ (Fig. 3.7b). The entire magnetic flux contained between the inner edge of the torus and the O-point is available for saturating the BH.

As we will see below, the initial condition (IC) described above and shown in Fig. 3.7a–d does contain a sufficient magnetic flux to saturate the BH with magnetic
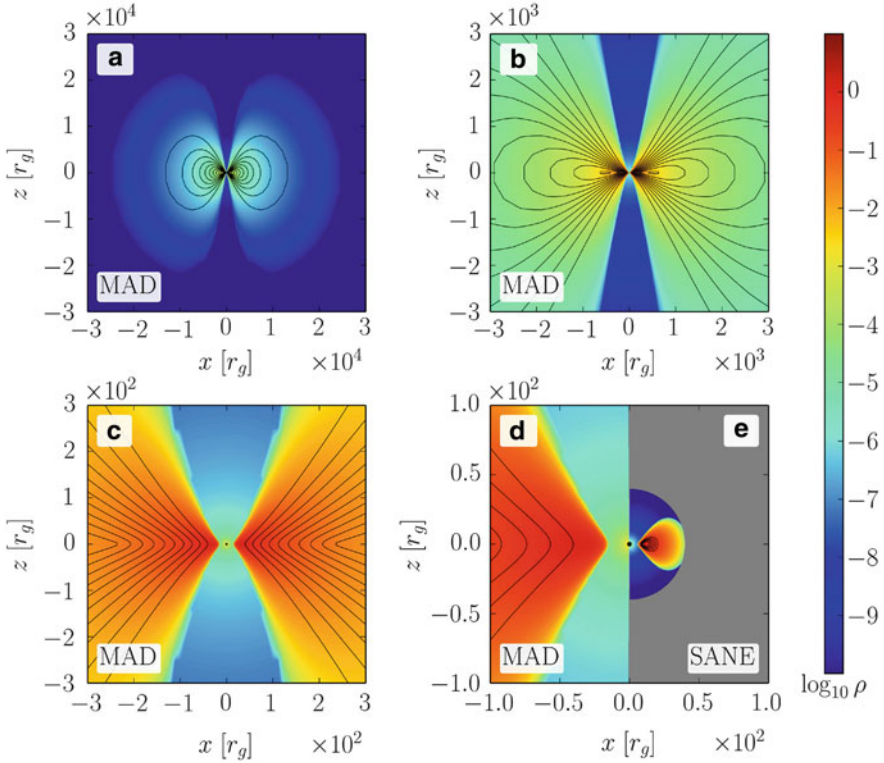
Fig. 3.7 A series of zooms into vertical slices through the simulation initial conditions (ICs). Color shows fluid-frame mass density ρ (*red* shows high and *blue* low values; see the color bar), *solid black lines* show poloidal magnetic field lines, and the *black circle* shows the BH. Panel (**a**): It is standard to initialize the simulations of BH accretion with a gas torus. This IC is similar, but the torus is chosen to be particularly large, allowing us to insert into it a magnetic flux large enough to readily flood the BH with magnetic flux and lead to a MAD. Hence, we call these "MAD" ICs. The computational domain extends out to Rout = $10^5 r_g$, i.e., to scales somewhat larger than the extent of the image. The magnetic field is weak, with $\beta = p_{gas}/p_{mag} \geq 100$, so it does not disturb the torus. Panel (**b**): A zoom-in on the MAD ICs. The O-point of the magnetic flux distribution is located at $r \simeq 600 r_g$, with all of the magnetic flux inside the O-point available for flooding the BH. Panel (**c**): A further zoom-in on the MAD ICs shows the large-scale magnetic flux of the same sign extends radially for more than an order of magnitude. Panel (**d**): This zoom-in on the MAD ICs shows the peak of the density distribution, which is located at $r_{max} = 34 r_g$, and the inner edge of the torus, which is located at $r_{in} = 15 r_g$. Panel (**e**): The standard ICs used in most simulations of BH accretion, the "SANE" ICs (this IC was generated by an open-source code HARM2D; see text for more details). They also start with a torus of gas threaded with a loop of weak magnetic field, but both the torus and the loop are much smaller than in the MAD ICs, as is apparent from the comparison to panel (**d**). For this reason, SANE ICs do not contain enough magnetic flux to readily flood the BH with magnetic flux. However, the magnetic flux is just a factor of few short of flooding the BH, highlighting the fine-tuned nature of such ICs (see Sect. 3.6). The computational domain extends out to $R_{out} = 40 r_g$, with the exterior of the computational domain shown in *gray color*

flux and lead to a MAD, and we will refer to this type of IC as the MAD IC. What is the main difference of this type of IC from the standard ICs used in general relativistic MHD simulations of BH accretion (De Villiers et al. 2003b; Gammie et al. 2003; McKinney and Gammie 2004; McKinney 2005; Hawley and Krolik 2006; Barkov and Baushev 2011)? Figure 3.7e shows an example of a standard IC, which is generated by the default setup of a freely available code HARM2D,[3] and which we will refer to as the SANE IC, which stands for "standard and normal evolution" (Narayan et al. 2012). It contains a much smaller magnetic flux than the MAD IC. The initial conditions of this type usually do not contain enough magnetic flux to reach the MAD state over the attempted duration of simulations. However, this is not always the case: for instance, Fig. 4 in Sądowski et al. (2013) shows that ϕ_{BH} in a SANE simulation for a BH with $a = 0.7$ slowly increases over time and eventually reaches $\phi_{BH} \sim 40$, i.e., the simulation enters the MAD state. In fact, any value of ϕ_{BH} between zero and $\sim$50 is possible in SANE simulations, and the value of ϕ_{BH} reached in any given simulation is determined by the initial distributions of large-scale magnetic flux and gas density. As we will see below, MADs reach $\phi_{BH} \sim 50$, essentially independent of initial conditions.

Clearly, the main difference between MAD and SANE ICs is the amount of available large-scale poloidal magnetic flux: it is much larger in the MAD ICs. Do we expect there to be a sufficient amount of large-scale magnetic flux in the environment of a supermassive BH to "flood" the hole with magnetic flux up to the MAD limit? How likely is it for such a flux to exist in a supermassive BH vicinity? Magnetic fields at the edge of the sphere of influence of a supermassive BH, i.e., $r \sim 100$ pc, are plausibly $B \sim \mu$G. Suppose these fields maintain their coherence over a roughly similar length scale. Does a patch of this size contain enough magnetic flux to make the central BH "go MAD" if the flux accretes down to the event horizon? Clearly, the magnetic flux contained in such a patch, $\Phi_{patch} \approx 10^{35}$ G cm^2, is much larger than the flux necessary to saturate a BH with magnetic field given by Eq. (3.14), $\Phi_{MAD} \approx 10^{33.5}$ G cm^2 (Narayan et al. 2003) (i.e., for a BH of mass $M_{BH} = 10^9 M_\odot$ accreting at $L = 0.1L_{Edd}$). It is thus plausible that MADs occur around supermassive BHs. Below we will see that there are observational indications that MADs are at work in a variety of astrophysical systems (see Sects. 3.7–3.10). Therefore, MADs are not rare or unusual as their name might imply, but in fact quite the opposite.

We carry out a simulation starting with our MAD IC shown in Fig. 3.7a–d. To maximize jet power, we consider a rapidly spinning BH, with $a = 0.99$. We carry out the simulations in 3D, using a numerical code HARM (Gammie et al. 2003; McKinney and Gammie 2004; Tchekhovskoy et al. 2007, 2009; McKinney and Blandford 2009; Tchekhovskoy et al. 2011; McKinney et al. 2012), which discretizes equations of general relativistic MHD in a conservative and shock-capturing form. We use the resolution of $288 \times 128 \times 64/128$ cells in $r-$, $\theta-$, and $\varphi-$directions, respectively (at $t \approx 15{,}000 r_g/c$ we double the $\varphi-$resolution from 64

---

[3]You can download the code at http://rainman.astro.illinois.edu/codelib

to 128 cells). The computational grid extends radially from $0.83r_H$ to $10^5 r_g$ and uses a logarithmically-spaced radial grid, $\Delta r \propto r$, near the BH. The θ-grid is adjusted so as to resolve both the collimating polar jets and the MRI in the equatorial disk. The φ-grid is uniform.

MAD Simulation Results The outcome of the simulation is shown in Fig. 3.8. This simulation as well as all other simulations discussed in this chapter, do not include any radiative losses or cooling, which is appropriate in geometrically-thick disks that are strongly sub-Eddington or super-Eddington (see Sect. 3.5). Figure 3.8a shows horizontal and vertical slices through the same IC as that shown in Fig. 3.7a–d. Figure 3.8e shows the rest mass energy flux into the BH, $\dot{M}(r_H)c^2$, as a function of time. Until a time $t \sim 2,000 r_g/c$, the MRI is slowly building up inside the torus and there is no significant accretion. After this time, $\dot{M}$ steadily grows until it saturates at $t \sim 4,000 r_g/c$. Beyond this time, the accretion rate remains more or less steady at approximately 10 code units until the end of the simulation at $t \sim 30,000 r_g/c$. The fluctuations seen in $\dot{M}$ are characteristic of turbulent accretion via the MRI.

Figure 3.8f shows the time evolution of the dimensionless magnetic flux ϕ_{BH} at the BH horizon. Since the accreting gas continuously brings in new flux, ϕ_{BH} continues to grow even after $\dot{M}$ saturates. However, there is a limit to how much flux the accretion disc can push into the BH. Hence, at $t \sim 6,000 r_g/c$, the flux on the BH saturates and after that remains roughly constant at a value around 50, with the flow near the BH being highly magnetized. Panel (b) shows that magnetic fields near the BH are so strong that they compress the inner accretion disc vertically and decrease its thickness near the BH down to $h/r \sim 0.05$; at larger distances the disk thickness settles to $h/r \approx 0.3$. The accreting gas, of course, continues to bring even more flux, but this additional flux remains outside the BH, obstructs gas inflow, and causes the disk to become a MAD (Tchekhovskoy et al. 2011; Narayan et al. 2003). Panels (c) and (d) show what happens to the excess flux. Even as the gas drags the magnetic field in, field bundles erupt outward (Igumenshchev 2008), leaving the time-average flux on the BH constant. For instance, two flux bundles are seen at $x \sim \pm 20 r_g$ in Fig. 3.8c which originate in earlier eruption events. Other bundles are similarly seen in Fig. 3.8d. During each eruption, the mass accretion rate is partially suppressed, causing a dip in $\dot{M}$ (Fig. 3.8e); there is also a corresponding temporary dip in ϕ_{BH} (Fig. 3.8f). Note that, unlike 2D (axisymmetric) simulations (e.g., Proga and Begelman 2003), there is never a complete halt to the accretion (Igumenshchev et al. 2003) and even during flux eruptions accretion proceeds via spiral-like structures, as seen in Fig. 3.8d.

The energy outflow efficiency shows considerable fluctuations with time (Fig. 3.8g), reaching values as large as $\eta \gtrsim 200\%$ for prolonged periods of time, with a long-term average value, $\langle \eta \rangle = 140 \pm 15\%$. This may explain sources with very efficient jets (McNamara et al. 2011; Fernandes et al. 2011; Punsly 2011). This value of efficiency is much larger (by a factor of $5-10$) than the maximum efficiencies seen in earlier simulations (McKinney 2005; Hawley and Krolik 2006; Barkov and Baushev 2011). The key difference is that, in our simulation, we
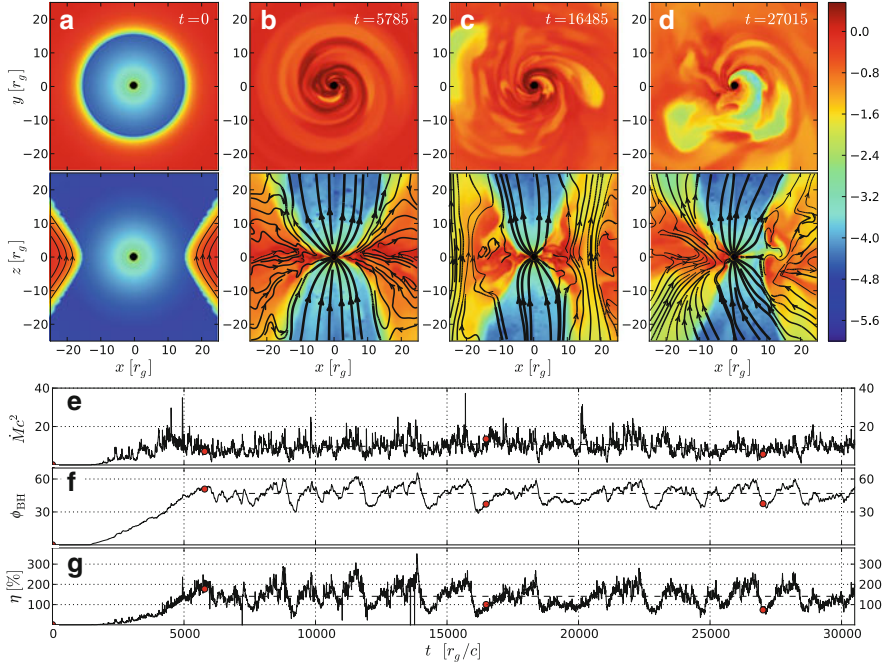
Fig. 3.8 Snapshots and time-dependence of in a simulation of a magnetically-arrested disk (MAD, taken from Tchekhovskoy et al. 2011), around a rapidly spinning BH, with $a = 0.99$. A movie is available at http://youtu.be/nRGCNaWST5Q. Panels (**a**)–(**d**): The *top* and *bottom rows* show, respectively, equatorial ($z = 0$) and meridional ($y = 0$) snapshots of the flow, at the indicated times. Colour represents the logarithm of the fluid frame mass density, $\log_{10} \rho$ (*red* shows high and *blue* low values; see colour bar), *filled black circle* shows BH horizon, and *black lines* show field lines in the image plane (the dominant, out-of-plane, magnetic field component is not shown; but see Fig. 3.9a). Panel (**e**): Time evolution of the rest-mass accretion rate, $\dot{M}c^2$. The fluctuations are due to turbulent accretion and are normal. The long-term trends, which we show with a Gaussian smoothed (with width $\tau = 1,500 r_g/c$) accretion rate, $\langle \dot{M} \rangle_\tau c^2$, are small (*black dashed line*). *Red dots* in the *three bottom panels* indicate the times of snapshots shown in the *top two rows* of panels. Panel (**f**): Time evolution of the large-scale magnetic flux, ϕ_{BH}, threading the BH horizon, normalized by $\langle \dot{M} \rangle_\tau$. At $t = 0$, the accretion flow contains a large amount of large-scale magnetic flux and there is zero flux on the BH. BH magnetic flux grows until $t \approx 6,000 r_g/c$. At this time the BH is saturated with magnetic flux. However, the accretion flow brings in even more flux, which impedes the accretion and leads to a magnetically arrested disk at $t \gtrsim 6,000 r_g/c$ (Panels (**c**) and (**d**) are during this period). Some of the flux escapes from the BH via magnetic interchange and flux eruptions, several of which are seen in panels (**c**) and (**d**), which frees up room for new flux. Panel (**g**) Time evolution of the energy outflow efficiency η (defined in Eq. 3.12 and here normalized to $\langle \dot{M} \rangle_\tau c^2$). During the initial stage of the simulation, $t \lesssim 6,000 r_g/c$, the power of outflows η grows, roughly proportional to ϕ_{BH}^2, as expected from Eq. (3.11). The strength of magnetic flux reaches saturation around $t \sim 6,000 r_g/c$ and the power of the outflow is maximum. During the subsequent quasi-periodic accumulation and rejection of magnetic flux by the BH, η fluctuates and its average value is $\eta \approx 140\%$. Since this exceeds 100%, the outflows carry more energy than the entire rest-mass energy supplied by accretion. This was the first demonstration of *net* energy extraction from a spinning BH in a realistic astrophysical setting

maximized the magnetic flux around the BH. This enables the system to produce a substantially more efficient outflow. Since $\eta > 100\%$, jets and winds carry more energy than the entire rest-mass supplied by the accretion. This is the first demonstration of *net* energy extraction from a BH in a realistic astrophysical scenario, a long sought result. Thicker MADs ($h/r \approx 0.6$) produce outflows at an even higher efficiency, $\eta \simeq 300\%$ (McKinney et al. 2012; Tchekhovskoy and McKinney 2012).

Note that Fig. 3.8 shows the magnetic field in the image plane, and the toroidal magnetic field component, B_φ, is not shown. As is clear from the 3D rendering of the accretion system shown in Fig. 3.9a, B_φ is actually the dominant component of the field in the jets. It can be seen from Fig. 3.9a that the jets extend out to much larger distances than the BH horizon radius and are collimated into a small opening angle by the disk wind.

Figure 3.8 shows that the accretion flow is highly time-variable and does not appear to resemble the idealized picture of regular magnetic field lines seen, for instance, in Fig. 3.3c. Does this mean that the simple, time-steady models are not at all applicable to the accretion simulations? To check this, let us average the accretion flow in time and in azimuth (i.e., in the φ-direction); the result is shown in Fig. 3.9b. Clearly, once the large-amplitude variability is averaged over, what is left is remarkably similar to the sketch shown in Fig. 3.3c.

Firstly, let us focus on the poloidal magnetic field lines, which are shown with black solid lines in Fig. 3.9b. They have the shape of a parabola, i.e., they curve up toward the polar regions as they move away from the BH. The group of field lines highlighted in green connects to the BH and makes up the twin polar jets. The jet field lines extract BH rotational energy and carry it away to large distances. These field lines have little to no gas attached to them and are therefore highly magnetized (since disk gas cannot cross magnetic field lines and is thus blocked from getting to the polar region, the jet field lines either drain the gas to the BH or fling the gas away by the rotation). The fact that a large amount of energy is coupled to these field lines but very little gas, allows them to accelerate efficiently to highly relativistic velocities. This acceleration occurs at distances much larger than the ones shown in Fig. 3.9b (Tchekhovskoy et al. 2008, 2009, 2010). As mentioned above, we denote the power of the jets as P_{jet}. The rest of the field lines, highlighted in blue, connect to the disk body and make up the magnetic field bundle that produces the slow, heavy disk wind. We denote its power as P_{wind}.

The flow of gas in Fig. 3.9b has the standard "hourglass" shape: part of the disk inflow turns around and forms the disk wind: disk wind streamlines originate in the disk body. Jet streamlines are connected to the BH. Note that in a time-average sense, disk flow streamlines cross magnetic field lines (i.e., red lines cross black lines): this would be impossible in axisymmetric ideal MHD. However, this is possible in 3D ideal MHD simulations because non-axisymmetric gas motions allow disk gas to go around magnetic field lines (e.g., via interchange instability). Note, however, that the disk wind streamlines do not cross into the jet boundary, i.e., no streamlines cross from the blue into green region: this is the reflection of suppressed turbulence and mixing in the polar regions.
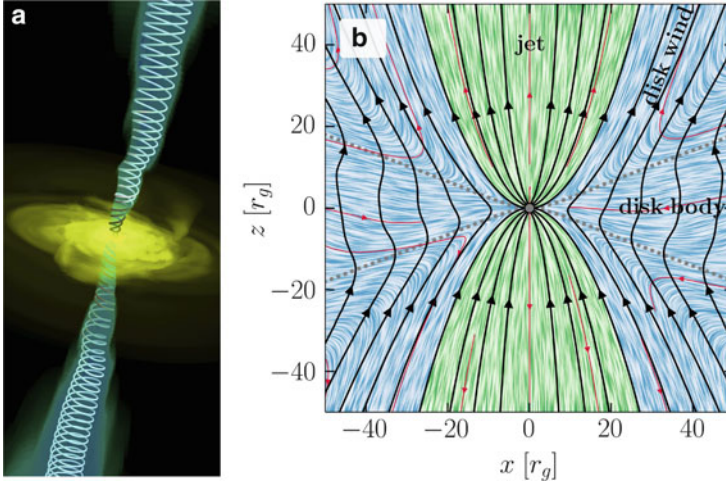
Fig. 3.9 Panel (**a**): A 3D rendering of our MAD $a = 0.99$ model at $t = 27,015r_g/c$ (i.e., the same time as Fig. 3.8d). Dynamically-important magnetic fields are twisted by the rotation of a BH (too small to be seen in the image) at the center of an accretion disk. The azimuthal magnetic field component clearly dominates the jet structure. Density is shown with color: disk body is shown with *yellow* and jets with *cyan-blue color*; we show jet magnetic field lines with *cyan bands*. The image size is approximately $300r_g \times 800r_g$. Panel (**b**): Vertical slice through our MAD $a = 0.99$ model averaged in time and azimuth over the period, $25,000r_g/c \leq t \leq 35,000r_g/c$. Ordered, dynamically-important magnetic fields remove the angular momentum from the accreting gas even as they obstruct its infall onto a rapidly spinning BH ($a = 0.99$). *Gray filled circle* shows the BH, *black solid lines* show poloidal magnetic field lines, and *gray dashed lines* indicate density scale height of the accretion flow, $|\theta - \pi/2| = h/r$. The symmetry of the time-average magnetic flux surfaces is broken, due to long-term fluctuations in the accretion flow. This is also seen from the streamlines of velocity, u^i, which we show in two ways: with directed *thin red lines* and with colored "iron filings", which are better at indicating the fine details of the flow structure. The flow pattern is a standard hourglass shape: equatorial *disk inflow* at low latitudes, which turns around and forms a *disk wind outflow* (labeled as "disk body" and "disk wind", respectively, and highlighted in *blue*), and twin polar *jets* at high latitudes (labeled as "jet" and highlighted in *green*). We show "iron filings" using *linear integral convolution* (LIC) method, which is available as a compilable Python module at http://wiki.scipy.org/Cookbook/LineIntegralConvolution; to increase the visual contrast of the LIC, we use the technique described at http://paraview.org/Wiki/ParaView/Line_Integral_Convolution#Contrast_enhancement

Whereas field lines in Fig. 3.3c show a sharp equatorial kink, it is not present in Fig. 3.9b. The kink occurs due to the simplifying assumption that the accretion disk and the electric current it carries are of a zero thickness, $h/r = 0$. However, in the simulation the disk thickness is finite, $h/r \approx 0.3$. This converts a singular equatorial current in Fig. 3.3c into a current sheet distributed over the disk thickness in Fig. 3.9b: most of the field line curvature is concentrated within the disk body, whose boundaries are approximately indicated by gray dashed lines defined by $|\theta - \pi/2| = h/r$.

Importantly, in the MAD state η is essentially independent of the initial amount of magnetic flux in the accretion flow, i.e., η depends only on BH spin, a, and disk density angular thickness, h/r (Tchekhovskoy and McKinney 2012). This allows us to reliably study spin-dependence of various quantities, shown in Fig. 3.10. Firstly, note that both prograde ($a > 0$; BH rotating in the same sense as the disk) and retrograde BHs ($a < 0$; BH is rotating in the opposite sense to the disk) have quite similar values of magnetic flux. We will focus on prograde BHs. The dimensionless BH flux, ϕ_{BH}, varies between 40 and 60 (Fig. 3.10a), with a characteristic value,

$$\text{In a MAD:} \qquad \phi_{\mathrm{MAD}} \approx 50. \quad \text{(spin-average)} \qquad\qquad (3.16)$$

Note that this is quite similar to our back of the envelope estimate of BH magnetic flux, Eq. (3.15). The spin-dependence of ϕ_{BH} can be approximated for $a \geq 0.3$ as

$$\text{In a MAD:} \qquad \phi_{\mathrm{MAD}} \approx 70(1 - 0.38\omega_{\mathrm{H}})h_{0.3}^{1/2}, \qquad\qquad (3.17)$$
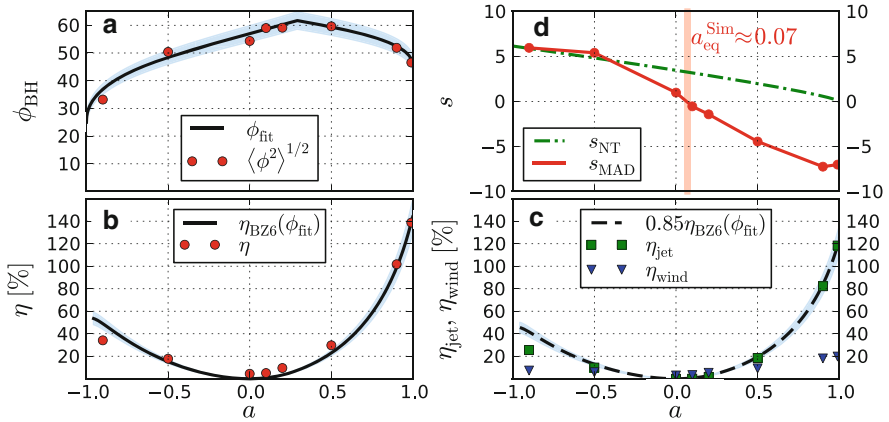

Fig. 3.10 Spin-dependence of various quantities for MADs with $h/r \approx 0.3$ (Taken from Tchekhovskoy et al. (2012)). Panel (**a**) Spin-dependence of dimensionless BH spin, ϕ_{BH}: *red dots* show simulation results, and the *black line* shows a by-eye fit, ϕ_{fit}, which is comprised of two linear segments in a ϕ_{BH}–Ω_{H} plane. *Blue bands* show a 5 % uncertainty on the fit. Panel (**b**) Spin-dependence of energy outflow efficiency, η: *red dots* show simulation results, *black line* shows the BZ6 approximation for efficiency (Eq. 3.7) assuming $\phi_{\mathrm{BH}}(a) = \phi_{\mathrm{fit}}(a)$, and the *blue band* shows the 10 % uncertainty on the fit. Panel (**c**) *Green squares* show jet efficiency η_{jet} and inverted *blue triangles* wind efficiency η_{wind}. *Dashed line* shows 85 % of the above BZ6 efficiency (a good estimate of jet power for prograde BHs (Tchekhovskoy and McKinney 2012)), and a *blue band* shows a 10 % uncertainty band. Panel (**d**) Connected *red dots* show spin-dependence of BH spin-up parameter in MAD simulations, s_{MAD} (see Eq. 3.20), and *green dash-dotted line* shows the spin-up parameter for a geometrically-thin Novikov-Thorne disk, s_{NT} (Novikov and Thorne 1973). Whereas for thin disks the equilibrium value of BH spin is $a_{\mathrm{eq}}^{\mathrm{NT}} = 1$, for MAD simulations it is much lower, is $a_{\mathrm{eq}}^{\mathrm{Sim}} \approx 0.07$, a value indicated by a *vertical red band*. Such a low equilibrium spin value results from a combination of two magnetic effects: (i) efficient extraction of BH spin energy by strong, dynamically-important magnetic fields threading the BH and (ii) removal of disc angular momentum by magnetized disk winds, so little angular momentum reaches the BH

where $h/r = 0.3h_{0.3}$. The corresponding BZ6 efficiency (see Eq. 3.7) is then

$$\text{In a MAD:} \qquad \eta_{\text{MAD}} \approx F(\omega_{\text{H}})h_{0.3} \times 100\,\% \approx 1.3h_{0.3}a^2 \times 100\,\%, \qquad (3.18)$$

where we used the fact that the spin-dependent factor entering jet power, $F(\omega_{\text{H}}) = 4.4\omega_{\text{H}}^2(1 - 0.38\omega_{\text{H}})^2 f(\omega_{\text{H}})$, can be approximated as $F \approx 1.3a^2$ to 10 % accuracy for $a \geq 0.3$, where $f(\omega_{\text{H}})$ is given by Eq. (3.8). The values of η for prograde and retrograde BHs are within a factor of a few of each other, suggesting that both of them can be responsible for producing powerful jets (Tchekhovskoy and McKinney 2012). The h/r dependence of ϕ_{MAD} and η_{MAD}, given in Eqs. (3.17) and (3.18), will be derived elsewhere. Panel (c) shows the division of total outflow efficiency into highly magnetized jet and weakly magnetized wind components, with efficiencies η_{jet} and η_{wind}, respectively. Jet efficiency at $a \gtrsim 0.2$ is well-approximated by:

$$\text{In a MAD:} \qquad \eta_{\text{jet}} \approx 0.65h_{0.3}a^2(1 + 0.85a^2) \times 100\,\%. \qquad (3.19)$$

Since jets are BH spin-powered (Eq. 3.7), for $a = 0$ jet efficiency vanishes, but winds still derive their power from an accretion disk via a Blandford-Payne–type mechanism (Blandford and Payne 1982). The larger the spin, the more efficient jets and winds. However, for rapidly spinning BHs most of the energy—about 85 % for prograde BHs—is carried by relativistic jets (Tchekhovskoy and McKinney 2012). Thus, for rapidly spinning BHs, the power of BH-powered jets exceeds by a factor of 5 the power of disk-powered winds, demonstrating that BH spindown power can dominate the total power output of an accretion system, which makes it plausible to use jets as diagnostic tools of the central BHs. This important result resolves a long-standing debate on the dominant source of power behind BH outflows (Ghosh and Abramowicz 1997; Livio et al. 1999). Importantly, even rather slowly spinning BHs, with $a \sim 0.5$, produce prominent BH spin-powered jets that outshine disk-powered winds.

Do our highly efficient jets affect the spin of central BHs? Figure 3.10d shows spin-dependence of BH spin-up parameter (Gammie et al. 2004),

$$s = \frac{M_{\text{BH}}}{\dot{M}} \times \frac{da}{dt}. \qquad (3.20)$$

If $s > 0$, the BH is spun-up by the sum of accretion and jet torques. If $s = 0$, BH is in spin equilibrium, i.e., its spin does not change in time. If $s < 0$, BH spin decreases. For standard geometrically thin accretion disks, $s > 0$, at all values of spin (see Fig. 3.10d and Novikov and Thorne 1973), and the equilibrium spin is $a_{\text{eq}}^{\text{NT}} = 1$ (Bardeen 1970) (we neglect photon capture by the BH, which would limit the spin to $a \approx 0.998$ Thorne 1974). Thick accretion flows in time-dependent

numerical simulations (McKinney and Gammie 2004; Gammie et al. 2004; Krolik
et al. 2005) typically have $a_{eq} \sim 0.9$. Figure 3.10d shows that the equilibrium value
of spin for our MADs (with $h/r \approx 0.3$) is much smaller, $a_{eq}^{Sim} \approx 0.07$, due to large
BH spin-down torques by the powerful jets. For example, in an AGN accreting at
$L = 0.1 L_{Edd}$, the central BHs would be spun down to near-zero spin, $a \lesssim 0.1$, in
$\tau \simeq 3 \times 10^8$ years. This value is interesting astrophysically because it is comparable
to characteristic quasar lifetime (but could be much longer than the duration of the
FRII phase of AGN). Over quasar lifetime, jets can extract a substantial fraction
of the central BH spin energy and deposit it into the ambient medium. The central
galaxy in the cluster MS0735.6+7421 can be one such example (McNamara et al.
2009).

How does the power of jets from MADs relate to previously reported results?
Figure 3.11 compares the approximation for η_{jet} in MAD simulations (given by
Eq. 3.19) to those for simulations using SANE ICs (McKinney 2005; Hawley and
Krolik 2006). Clearly, MADs produce much more powerful jets than found in
previous work, by a factor 5–10, depending on the value of the spin. This is not
surprising because MADs achieve the maximum possible amount of magnetic flux
threading the BH and thus achieve the maximum possible jet power: for fixed BH
spin and $\dot{M}$, any SANE simulation will have jet power *below* that of a MAD. On
the other hand, a deficit by a factor of 10 in jet power translates into a deficit by a
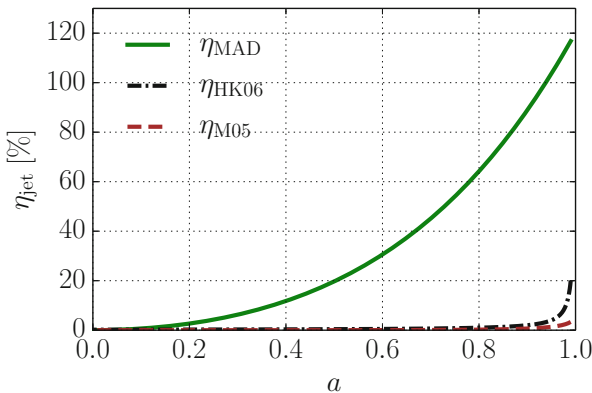factor of ~ 3 in magnetic flux. This means that the magnetic flux in SANE initial

Fig. 3.11 Comparison of jet energy production efficiency obtained in MAD simulations, η_{jet} (due
to Eq. 3.19), which is shown with *green solid line*, with previously reported approximations of
simulated jet power: HK06, which is shown with *black dash-dotted line* (Hawley and Krolik 2006),
and M05, which is shown with *brown dashed line* (McKinney 2005), plotted over the range $0 \leq
a \leq 0.99$. Clearly, MADs produce much more efficient jets than in previous work: this is not
surprising because for a given $\dot{M}$, MADs have the maximum possible amount of magnetic flux
threading the BH and thus achieve the maximum possible jet power. Note that the shape of the
spin-dependence of jet power is different in MAD simulations than in previous work, suggesting
that the dependence of jet power on BH spin in SANE simulations is affected by the distribution
of gas and magnetic flux in the initial conditions

conditions is *tuned* to be just a factor of few below the MAD ICs. Therefore, a mere increase of magnetic flux by $\gtrsim 3\times$ would cause SANE simulations to "go MAD". That SANE simulations did not become MAD is a consequence of the particular choice of initial torus size, magnetic flux distribution, and potentially limited run time. In fact, some SANE simulations eventually "go MAD", as we discussed when we first introduced SANE ICs.

3.7 Correlation of Jet Power and BH Spin for Stellar-Mass BHs

For a while astrophysicists have been able to measure the masses of BHs in AGN and BHBs. However, only in the past decade have they been able to reliably measure the spins of the BHs. There are two major methods of BH spin measurement. Both methods operate best when the accretion disk is close to the geometrically-thin disk state (Fig. 3.5b), which is the best understood of all BH accretion states. Both of the methods rely on the fact that disk emission cuts off (Shafee et al. 2008; Penna et al. 2010; Kulkarni et al. 2011; Zhu et al. 2012) inside the *innermost stable circular orbit*, or ISCO, whose radius has a monotonic, strong dependence on BH spin: $r_{\rm ISCO} = r_g$ for maximally spinning BHs (with $a = 1$) and $r_{\rm ISCO} = 6r_g$ for non-spinning BHs (with $a = 0$; see, e.g., Shapiro and Teukolsky 1986). By measuring the radius of the "hole in the disk", or $r_{\rm ISCO}$, one can then determine the BH spin.

In the continuum fitting method the radius of the ISCO is found via the analysis of the continuum black-body–like emission from the inner disk (see McClintock et al. 2011, 2013 for a recent review). On a qualitative level, since most of the disk emission is produced in a ring of radius $\simeq r_{\rm ISCO}$, the emergent luminosity is given by $L \sim \pi r_{\rm ISCO}^2 \sigma T^4$, where σ is Stephan-Boltzmann constant and T is the blackbody temperature of the inner disk. By measuring L from the normalization of the X-ray spectrum and T from the shape of the spectrum, one can then solve for $r_{\rm ISCO}$ and a. The iron line method relies instead on analyzing the shape of iron emission lines (as well as other "reflection" features), which are good tracers of inner disk dynamics: the red wing of the iron line profile is sensitive to the position of disk inner edge and thus its modeling allows one to measure BH spin (see Fabian et al. 2000; Reynolds 2013a for an introduction).

If it is the central BHs that power the jets, we would expect jet efficiency to correlate with BH spin. While there is no evidence for such a correlation for continuous jets in stellar-mass BHs (Fender et al. 2010), recently such a correlation was found for transient stellar-mass BH jets (Narayan and McClintock 2012). Whereas jet power cannot be measured directly, one can measure its proxy, radio emission, or more specifically, the luminosity at 5 GHz radio frequency, $L_{\rm 5\,GHz,peak}$, at the peak of its emission. Note that, we are interested not in jet power but in jet energy efficiency η. In order to find it, we would need to divide jet power by mass accretion rate $\dot{M}$. However, $\dot{M}$ is difficult to measure for transient events. Instead,

one can make use of the fact that state transitions often behave as "standard candles": mass accretion rate reaches an order unity fraction of Eddington luminosity at its peak during the state transition and is thus proportional to BH mass M. Thus, an observational proxy for jet efficiency is $\eta_{obs} \propto L_{5GHz,peak}/M$, and we expect this quantity to correlate with BH spin. Indeed, a correlation between η_{obs} and a is observed and shown in Fig. 3.12 (but see Russell et al. 2013).

This correlation is consistent with the picture that transient jets are powered by magnetically-extracted BH spin energy. This correlation also implies that different BHs are filled with magnetic flux to the same degree, i.e., that they have similar values of the dimensionless magnetic flux ϕ_{BH}. This could be understood if the production of most transient jets is accompanied with the formation of a MAD, when ϕ_{BH} saturates at the maximum possible value. In some cases, however, there can be an insufficient amount of magnetic flux to saturate the BH and lead to a MAD. Such sources would fall below the correlation shown in Fig. 3.12, so it is possible that the correlation gives *an upper envelope* of jet power. If so, then the correlation translates a measurement of jet power into a *lower limit* on BH spin. A robust correlation between jet power and BH spin is an extremely useful tool since
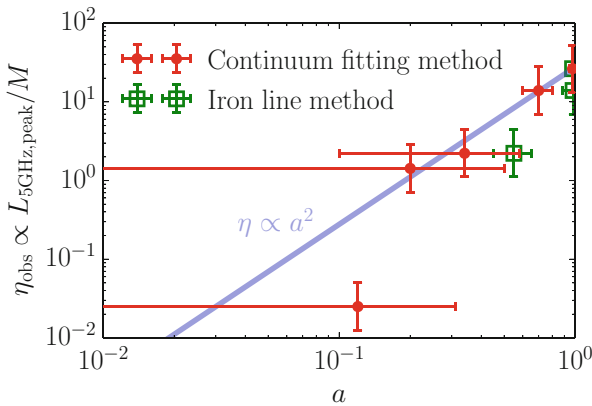

Fig. 3.12 Observational evidence for a correlation between the power of transient BHB jets and BH spin (using the updated data set from Steiner et al. 2013; see also Narayan and McClintock 2012). This figure plots spin versus a proxy for transient jet power, the 5 GHz radio luminosity $L_{5\,GHz,peak}$. Jet power has been corrected for beaming assuming a Lorentz factor $\Gamma = 2$, and normalizing by BH mass M to obtain jet efficiency (see the text for those details). Retrograde spins are not considered here, and sources with poorly constrained inclinations have likewise been omitted. BH spin was measured using the continuum fitting (shown with *red circles*) and iron line (shown with *open green squares*) methods. Jet power increases with increasing BH spin a. The *blue solid line* shows a quadratic dependence $\eta \propto a^2$ that is consistent with the data. If this curve gives the upper envelope of jet power, one expects all X-ray binaries to fall *under* this curve. The data is shown, from low-to-high η_{obs}, for A0620–00, H1743–322, XTE J1550–564, GRO J1655–40, and GRS 1915+105. Error bars on the spin are 1-σ. As illustrated in the figure, the two spin measurement methods generally agree to within 1-σ error. Error bars on the jet power are taken to be a factor of 2

it allows one to convert a relatively easy measurement of jet power into a hard-to-measure value of BH spin, as was recently demonstrated (Steiner et al. 2013).

3.8 Microquasars as "Quasars for the Impatient"

Jet-producing AGN fall into two classes (Fanaroff and Riley 1974): (i) low-luminosity AGN that produce jets whose emission is centrally-dominated (so-called FRI sources, e.g., M87 galaxy) and (ii) high-luminosity AGN that produce jets whose emission is dominated by a pair of hot lobes in which the twin jets interact with the ambient medium (so-called FRII sources, e.g., Cygnus A galaxy). If an FRI jet points toward us, it appears as a *BL Lac* object, whereas if an FRII jet points at us, it appears as a *blazar* (see Urry and Padovani 1995 for a review). Both of these classes of sources are referred to as *radio-loud* AGN.

As we discussed in Sect. 3.1, it is compelling to identify a single mechanism responsible for producing jets across the entire mass range of BHs, i.e., both stellar-mass BHs in BHBs and supermassive BHs in AGN. It is appealing to think of stellar-mass BHs as scaled-down supermassive BHs, or "quasars for the impatient" (Blandford 2005).

However, when we try to draw such an analogy, we run into apparent difficulties. In BHBs, there is clear evidence that geometrically-thin disks do not produce any jets or associated radio emission (see, e.g., Russell et al. 2011). However, detections of a "big blue bump" in the spectra of some blazars (Tavecchio et al. 2011; Cowperthwaite and Reynolds 2012) seemingly indicate the presence of a geometrically-thin accretion disk and imply that—in contrast to stellar-mass BHs—supermassive BHs with geometrically-thin disks are capable of producing jets! Does this mean that there is really a fundamental difference in the physics of jet production between stellar-mass and supermassive BHs and that no useful analogies between the two BH populations can be drawn?

Let us make an attempt to sort things out. FRI jets are clear analogs of continuous BHB jets: both occur at low accretion luminosities, $L \lesssim 0.01 L_{\mathrm{Edd}}$. FRII jets are much more powerful than FRI jets, and it is less clear what their stellar-mass analogs are. There are, however, not many candidates to choose from.

Could transient stellar-mass BH jets—these are the same jets that appear during hard-to-soft accretion disk spectral state transitions and that we discussed in Sect. 3.5—be the low-mass analogs of FRII jets (Sera Markoff, private communication; see also van Velzen and Falcke (2013))? Indeed, just like FRII jets are more powerful than FRI jets, transient jets are more powerful than the continuous jets. Also, both FRII jets and transient jets appear over roughly the same luminosity range, $L \sim (0.01-1) L_{\mathrm{Edd}}$ (see, e.g., Sikora et al. 2007; Fender et al. 2004).

According to this analogy, FRII objects are in a "transient" evolutionary phase of AGN. During this phase they transition from being FRI AGN to becoming jet-less

quasars. If the characteristic duration of state transitions scales linearly with central BH mass, this phase lasts 10^4-10^7 years in AGN (see Sect. 3.5). What happens to the inner regions of the accretion disk during this transition? In analogy with BHBs, mass accretion rate increases to a substantial fraction of Eddington. This increase is accompanied with the change in the state of the inner accretion disk: it switches from a radiatively-inefficient sub-Eddington accretion flow in FRI stage (Fig. 3.5c) to a radiatively-efficient geometrically-thin accretion flow in the quasar stage (Fig. 3.5b).

Realization that FRII jets and transient BHB jets are the same physical phenomenon, only occurring on different mass scales, resolves the puzzle that we started with: the detections of "big blue bump" emission in the spectra of blazars *do not* imply that their accretion disks are canonical geometrically-thin accretion disks. In contrast, these are perturbed disks in the process of changing their identity. In fact, the spectra of stellar-mass BHs undergoing the hard-to-soft spectral state transition also show a blackbody-like component whose strength increases as the transition progresses (Fender et al. 2004), reflecting the underlying change from a geometrically-thick to geometrically-thin disk. In fact, the inner edge of the geometrically-thin disk appears to *move inward* as the state transition progresses, reflecting a "refilling" geometrically-thin disk (Fender et al. 2004). This might be precisely what is observed in a blazar 3C120 (Cowperthwaite and Reynolds 2012).

Recently van Velzen and Falcke (2013) reported a tight correlation, for a sample of FRII AGN, between the radio lobe luminosity (which is expected to trace jet power) and the optical luminosity (which is expected to trace mass accretion rate). In fact, this correlation was so tight that the authors concluded that FRII jets could not be powered by BH spin: any conceivable spread in BH spin distribution would have led to scatter in jet power in excess of the observed one. However, an alternative explanation is equally plausible: that most of the BHs are near maximally spinning. To resolve this puzzle, it would be extremely useful to obtain independent measurements of BH spins of jet-producing BHs. However, these are difficult to come by because the accretion disk during the state transition is strongly perturbed away from the standard thin disk state. Indeed, most of the supermassive BH spin measurements have been performed for jet-phobic BHs that accrete via standard thin disks (Reynolds 2013b), and these measurements suggest that many jet-phobic supermassive BHs are rapidly spinning. If jet-producing AGN represent a relatively short phase of an AGN lifecycle, both jet-producing and jet-phobic supermassive BHs share the same BH spin distribution. Hence, it is conceivable that most jet-producing supermassive BHs are rapidly spinning as well, thereby resolving the puzzle. It is also possible that the optical luminosity is contaminated by jet emission and thus naturally strongly correlates with the jet power, so the detected correlation is between radio and optical emission *from the same jet* and does not tell us anything about the disk-jet connection.

3.9 MADs in Radio-Loud AGN

In Sect. 3.8 we argued that jets in blazars are supermassive analogs of transient jets in stellar-mass BHs. According to this analogy, if transient jets are powered by MADs (see Sect. 3.7), we expect the jets in blazars and FRII AGN to be powered by MADs as well. How can we test this hypothesis observationally? One way is to measure the jet power $P_{\rm jet}$ and compare it to accretion power $\dot{M}c^2$: if we robustly find $P_{\rm jet} \geq \dot{M}c^2$, this is an indication that MADs power these jets. Many studies point toward an approximate equality between jet and accretion powers (Rawlings and Saunders 1991; Ghisellini et al. 2010; Fernandes et al. 2011; McNamara et al. 2011; Punsly 2011; Martínez-Sansigre and Rawlings 2011). One of the most robust ways of constraining jet efficiency is to measure jet power $P_{\rm jet}$ from the energetics of X-ray emitting cavities inflated by the jets and divide it by mass-energy accretion rate $\dot{M}_{\rm B}c^2$ measured from the density of X-ray emitting gas within the sphere of influence of the BH called the Bondi radius, $r_{\rm B} \sim 10^5 r_g$. This gives quite a low efficiency of jet production (Allen et al. 2006). However, if one accounts for the gas expelled from the disk by its wind, we find that $\dot{M}$ near the BH is much lower than $\dot{M}_{\rm B}$. Jet efficiency then is well above 100 % for a sample of nearby low-luminosity AGN, suggesting that they are powered by MADs (Nemmen and Tchekhovskoy 2014).

We can also try and directly measure magnetic field strengths threading the central supermassive BHs. One way to do so is through Faraday rotation, which is the rotation of polarization plane of emission as it propagates through magnetized gas. For a recently discovered radio source in the vicinity of the supermassive BH at the center of our Galaxy, SgrA*, this gives a field strength of $B \sim 8\,{\rm mG}$ at a distance $r \sim 10^5 - 10^7 r_g$ from central BH (Eatough et al. 2013). Assuming the radial scaling $B \propto r^{-1}$, one arrives at an estimate of magnetic field at the BH horizon, $\simeq$ few $\times\,100\,{\rm G}$, which is close to the maximum possible magnetic field on the BH, as given by the estimate (3.14).

Such magnetic field measurements are quite difficult to come by for supermassive BHs in other galaxies, where there is a paucity of linearly polarized background radio sources close to the central nucleus that are bright enough for Faraday rotation measurement to be feasible. In order to find out if dynamically-important magnetic fields are an outlier or a norm for supermassive BHs, we need to measure field strengths near many of them. For this, we need to change our strategy. Instead of getting a handle on the magnetic field strength in accretion disks, we can measure it in the jets. One way of doing so is via a *core-shift* method. It focuses on jet's photosphere, which is the surface at which the jet becomes transparent to its own synchrotron radiation and which appears as a bright radio-emitting feature called the *radio core*. The distance from the BH to the *core* is of order $r_{\rm core} \sim 10^3 r_g$ and depends in a well-understood way on both the jet magnetic field strength *and* the observational frequency. By measuring the distance $\Delta r_{\rm core}$ between the positions of the core at two adjacent frequencies, or the *shift*, one can obtain the field strength in the frame of the jet, $B'_{\rm core} \propto \Delta r_{\rm core}^{3/4}$ and, after some manipulation, the magnetic flux

through the jet, Φ_{jet}. The luminosity of the accretion flow gives the mass accretion rate, $\dot{M} = L_{acc}/\epsilon c^2$, where one adopts a characteristic disk radiative efficiency for a rapidly spinning BH, $\epsilon \approx 0.4$. Now we are in a position to compute the prediction for the maximum possible value of magnetic flux that a BH can hold, $\Phi_{MAD} = 50G(\epsilon c^5)^{-1/2}L_{acc}^{1/2}M$ (see Eqs. 3.10 and 3.16), which is shown in Fig. 3.13 with the dashed line. As is clear from Fig. 3.13, the measured values of Φ_{jet} agree with the MAD prediction over seven orders of magnitude in L_{acc}. This suggests that the central BHs of these AGN are threaded with dynamically important magnetic field and their accretion disks are in the MAD regime.

Thus, the accretion disks in radio-loud AGN are *not* standard geometrically-thin accretion disks. This is a key difference from jet-less quasars, which most likely contain standard geometrically-thin accretion disks and hence are incapable of producing jets. This may resolve the apparent puzzle that most quasars, for which central BH spins have been measured, do not produce jets even though their central BHs tend to be rapidly spinning (Reynolds 2013b).
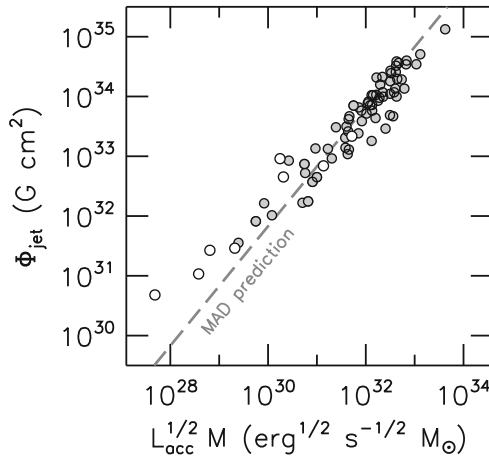

Fig. 3.13 Measured jet magnetic flux, Φ_{jet}, versus $L_{acc}^{1/2}M$, where L_{acc} is the luminosity of the accretion flow and M is BH mass (Taken from Zamaninasab et al. (2014)). The observational data for Φ_{jet} is shown with *open circles* for BL Lacs and *filled circles* for blazars. It is consistent with the MAD prediction for the magnetic flux on the BH, which is shown with the *dashed line* (see text for details). This suggests that the central BHs of radio-loud AGN—including blazars and BL Lacs—are threaded with dynamically-important magnetic fields and accrete surrounding gas in the MAD regime. The MAD prediction is computed assuming a radiatively efficient accretion flow with efficiency $\epsilon = 0.4$, which is appropriate for rapidly spinning BHs. As expected, BL Lac points are systematically shifted to the left of the correlation because their disks are radiatively inefficient

3.10   MADs in Tidal Disruption Events and Gamma-Ray Bursts

So far we discussed evidence for MADs in BHBs and radio-loud AGN. In fact, it is likely to find a MAD in essentially *any* BH accretion system whose mass accretion rate decreases asymptotically to zero. The reason for this is simple. Suppose an accretion flow contains a small but nonzero amount of large-scale magnetic flux. The flow drags this flux into the BH, so the strength of BH magnetic flux increases in time until nearly all of the flux ends up threading the BH. However, even as the BH magnetic flux increases, the mass accretion rate decreases in time. Therefore, it is inevitable that after some time BH magnetic flux becomes dynamically important, and a MAD forms. We will now discuss two examples of such transient systems—tidal disruption events (TDEs) and gamma-ray bursts (GRBs)—and the observational manifestations of their MADs.

MADs in Tidal Disruption Events An unfortunate star that passes too close to a supermassive BH and becomes tidally disrupted by the hole's gravity offers a unique probe of general relativity and accretion physics. As the star is torn apart by BH tidal forces, about half of its material becomes bound to the BH, forms an accretion disk and produces an optical, UV, and X-ray flare lasting for months to years (Ulmer 1999). Recently, two X-ray/soft gamma-ray events detected by the *Swift* observatory, Sw J1644+57 (Bloom et al. 2011; Burrows et al. 2011; Zauderer et al. 2011) and Sw J2058+05 (Cenko et al. 2012), have been associated with such TDEs. The association is based on the close proximity of the flare to the center of the host galaxy (and thus the central supermassive BH) and on the X-ray light curve time-dependence, $L_X \propto t^{-5/3}$, as seen in Fig. 3.14 and theoretically expected during a TDE for the mass fallback rate $\dot{M}_{fb}$ (Rees 1988) and BH mass accretion rate, $\dot{M}$, which is plausibly a fraction of $\dot{M}_{fb}$. However, unlike the usual TDEs, here the observed X-ray emission is believed to be produced by a relativistic collimated magnetized jet with an opening angle $\theta_j \sim 0.1$ radians. This is based primarily on the highly super-Eddington nature of the event, $L_X/L_{Edd} \sim 100$, as shown in Fig. 3.14 on the right $y-$axis,[4] and the detection of a radio afterglow due to a collimated jet running into the ambient medium (Giannios and Metzger 2011; Zauderer et al. 2011, 2013; Metzger et al. 2012; Berger et al. 2012; Wiersema et al. 2012).

It is highly likely that a stellar orbit was mis-aligned relative to BH midplane, since a star approaching the BH toward its death from a large distance did not know about BH's spin direction. However, there is no observational indication of such a misalignment: if the stellar orbit were misaligned, we would expect the resulting accretion disk to be misaligned as well. Such disks undergo precession around the BH (see, e.g., Fragile et al. 2007). If the direction of the jets follows the disk, the jets

---

[4]We do not expect disk luminosity to exceed L_{Edd} by more than a factor of a few, but there is no such constraint on jet luminosity.

would process as well. However, this is ruled out: after the initial flaring ended, the X-ray emitting jet appeared to point steady at us, with no sign of strong precession (Stone and Loeb 2012). Does this mean that we were extremely lucky and the stellar orbit was nearly perfectly aligned with BH midplane? Not necessarily! In tilted disk-jet systems, the formation of a MAD causes the jets to reorient along BH spin axis (McKinney et al. 2013); thus, dynamically-important magnetic fields can provide the required stability of jet orientation in Sw J1644+57 without fine-tuning.

One of the most surprising features of Sw J1644 light curve, is the extremely strong early-time variability, or "flaring", seen in Fig. 3.14 during the first ∼10 days. If BH spin axis points at us and the stellar orbit is tilted, the jets reorient along the BH spin axis only after the MAD forms. However, this reorientation is not instantaneous nor is it clean: as the jets work to reorient themselves, they punch holes through the disk and undergo a period of intense wobbling (McKinney et al. 2013). During this period, every time a jet passes in front of us, its emission beams into our line of sight, and we see a flare. This jet rearrangement process can naturally explain the initial period of strong flaring in the X-ray light curves of Sw J1644+57 (Tchekhovskoy et al. 2014). Moreover, prior to the MAD formation, the jets are misaligned, and their X-ray emission is beamed away from us, suggesting that the
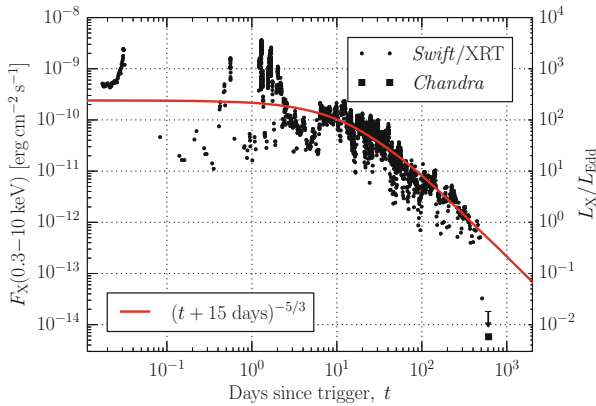

Fig. 3.14 X-ray lightcurve of the jetted tidal disruption event, Sw 1644+57, vs the time since *Swift*'s gamma-ray trigger (Adapted from Tchekhovskoy et al. (2014)). *Black dots* and the upper limit show data from the XRT telescope on board the *Swift* satellite, and the *black square* shows data from the *Chandra* X-ray observatory. The light curve shows several features: (i) the early-time "plateau" stage at $t \lesssim 10$ days, during which the X-ray luminosity is strongly variable but is on average constant, (ii) power-law decline stage, in which the light curve is consistent with the standard scaling expected for mass fallback rate in a TDE, $L_X \propto t^{-5/3}$, (iii) abrupt jet shutoff at $t \sim 500$ days. If we associate the jet shutoff with the spectral state transition ($a \to c$ in Fig. 3.5) from super-Eddington jet-producing accretion disk to jet-phobic standard geometrically-thin disk, which occurs at $\dot{M} \lesssim \dot{M}_{edd}$, we can infer the mass accretion rate shown on the right y−axis in Eddington units. We see that the accretion flow starts out highly super-Eddington. Apart from the variability, the light curve is consistent with a single power-law dependence, whose zero-point by $\sim 15^{+15}_{-7}$ days precedes the trigger, $L_X \propto (t + 15 \text{ days})^{-5/3}$ (see text for more details)

central BH was active for some time before the trigger. Indeed, an entire light curve, apart from the flaring, can be fit by a single power-law that starts 15^{+15}_{-7} days before the trigger, e.g., by $L_{jet} \propto (t + 15 \, \text{days})^{-5/3}$, as shown with the solid red line in Fig. 3.14 (see Tchekhovskoy et al. 2014 for details).

The presence of a MAD also explains why the jet luminosity L_{jet} (which we assume makes up a fixed fraction of P_{jet}) follows the power-law scaling that is expected for a mass accretion rate $\dot{M} \propto \dot{M}_{fb} \propto t^{-5/3}$. This is because MADs naturally give $P_{jet} \propto \dot{M}$ (see Figs. 3.8 and 3.10). Absent a MAD, obtaining such a scaling is non-trivial: P_{jet} is set by the large-scale magnetic flux threading the BH (see Eq. 3.7), which in general is independent of $\dot{M}$ (Tchekhovskoy et al. 2014), and below we consider an example of such a system.

MADs in Gamma-ray Bursts What other astrophysical systems have decreasing $\dot{M}$? Essentially, any transient system. Note that nearly all systems that we have discussed so far in the context of MADs are transient systems: (i) outbursts of BHBs accompanied by transient jets, (ii) outbursts of AGN accompanied by FRII jets, (iii) outbursts of AGN powered by TDEs. Another important system of this type is a core-collapse gamma-ray burst (GRB), in which a massive star ends its life, the stellar core collapses into a BH,[5] and the rest of the star accretes on to the BH with a steep dependence of mass-accretion rate on time, $\dot{M} \propto t^{-3}-t^{-20}$ (Woosley 1993; MacFadyen and Woosley 1999; Popham et al. 1999). The BH powers a pair of ultra-relativistic jets that emerge out of the star and produce the GRB, an energetic burst of gamma-rays that is detectable if one of the jets happens to point at us. However, here lies a puzzle: if a jet is characterized by a constant energy efficiency, its power would decrease proportionally to $\dot{M}$: $P_{jet} \propto \dot{M}$. But that is not what is observed: gamma-ray luminosity, or jet power, apart from random fluctuations, remains constant for most of the burst, $10-100$ s, and then abruptly declines. This sudden drop at the end of the GRB is called the *steep power law decline*.

What causes such a rapid change in jet power? At the start of the burst, magnetic fields are not dynamically-important, or else they would lead to GRB luminosity far in excess of what is observed ($B_{MAD} \sim 10^{17}$ G, whereas observationally $B_{BH} \lesssim 10^{15}$ G). The power of the jets is limited by the stellar magnetic flux collected on the BH by accretion, i.e., at the early time the jet power is roughly constant. However, as $\dot{M}$ decreases, MAD eventually forms: BH magnetic flux becomes dynamically-important and leaves the BH, with jet power dropping precipitously, $P_{jet} \propto \dot{M} \propto t^{-3}-t^{-20}$. This provides a natural explanation for the origin of the steep power law decline of GRB light curves (Tchekhovskoy and Giannios 2014).

---

[5]It is also possible that instead of the BH, a NS with strong magnetic fields, or a magnetar, powers the GRB.

Discussion and Conclusions

We started this chapter with describing a Blandford-Znajek process by which a large-scale poloidal magnetic field extracts and carries away BH rotational energy. The Blandford-Znajek mechanism is a very attractive source of power for jets as it works equally well for BHs of all sizes, stellar-mass and supermassive BHs. Over most of the range of BH spin ($a \lesssim 0.95$), the expression for power of Blandford-Znajek powered jets is very simple: $P_{\text{jet}} \propto \Omega_H^2 \Phi_{\text{BH}}^2$ (Eq. 3.6), where Ω_H is BH angular frequency and Φ_{BH} is the poloidal magnetic flux threading the BH.

Because of the freedom in Φ_{BH}, for a fixed value of BH spin a and mass accretion rate $\dot{M}$ we expect a range of jet powers from zero (no jet) up to a maximum value of power at which the BH magnetic flux is so strong that it stops gas infall: this value of flux is approximately $\Phi_{\text{MAD}} \approx 50(\dot{M} r_g^2 c)^{1/2}$ (see Eqs. 3.10 and 3.16). Such a strong magnetic flux leads to the formation of a *magnetically-arrested disk*, or a MAD. Since the BH magnetic flux is maximum in the MAD state, MADs achieve the maximum possible efficiency of jet production, $\eta_{\text{jet}} = (P_{\text{jet}}/\dot{M}c^2) \times 100\,\%$ that exceeds 100 % for rapidly spinning BHs (see Sect. 3.6 for details). Thus, MADs around rapidly spinning BHs perform *net* energy extraction from a rotating BH in a realistic astrophysical scenario, a long-sought result. Hence, it is not surprising that jet efficiency of MADs is much higher than the previously reported simulation results, $\eta_{\text{jet}} \lesssim 20\,\%$ (e.g., McKinney 2005; De Villiers et al. 2005; Hawley and Krolik 2006; Barkov and Baushev 2011).

MADs produce powerful jets that extract BH spin energy so efficiently that a BH accreting at 10 % of the Eddington rate spins down to near zero spin in $\simeq 3 \times 10^8$ years, a time scale comparable to the quasar life time. This suggests that jets can extract a substantial fraction of BH spin energy, provide substantial feedback on the environment of the supermassive BH, and affect galaxy evolution.

However, not all accreting BHs produce jets. We reviewed different spectral states of BH accretion disks and their ability to launch relativistic jets in Sect. 3.5. We saw that continuous jets are launched at high, $L \gtrsim L_{\text{Edd}}$, and low, $L \lesssim 0.01 L_{\text{Edd}}$, accretion luminosities, both by stellar-mass and supermassive BHs. Transient jets from stellar-mass BHs are launched in the intermediate luminosity range, $L \sim (0.01-1)L_{\text{Edd}}$. This range is similar to the one for FRII AGN jets, and we suggest that FRII jets are the supermassive analogs of transient jets in stellar-mass BHs. Following this analogy, we argued that the disks in FRII AGN are perturbed, *transient* disks in the process of changing their identity, similar to the transient disks in stellar-mass BHs during spectral state transitions (Sect. 3.8).

Standard geometrically-thin disks exist in the same luminosity range as the transient stellar-mass BH disks, $L \sim (0.01 - 1)L_{\mathrm{Edd}}$, but do not produce jets or associated radio emission. What makes transient disks and standard thin disks so different from each other if they have the same value of $\dot{M}$? Recently, magnetic field strength threading supermassive BHs was measured, and it was found that the central BHs of many radio-loud AGN are accreting in the MAD regime (Zamaninasab et al. 2014). It is thus plausible that transient disks contain much stronger large-scale magnetic flux than the standard geometrically-thin disks (Sects. 3.7 and 3.9). This strong magnetic flux obstructs gas infall, modifies the nature of accretion, and leads to strong jets. MADs have also been inferred in tidal disruption events and core-collapse gamma-ray bursts (Sect. 3.10).

If BH accretion in the MAD regime is common, in many astrophysical systems the strength of BH magnetic flux is constrained by the dynamics of the accretion flow (see, e.g., Eq. 3.16) and is not a free parameter. This, for the first time, opens the possibility of modeling accreting BHs with 0 (*zero*) variables that parametrize our ignorance of physics. Thus, specifying just three physical parameters—M_{BH}, a, and $\dot{M}$—is sufficient to completely define a simulated MAD system.[6] With the advent of global simulation methods that self-consistently account for radiation feedback on the structure and dynamics of accretion flow (Sądowski et al. 2014; McKinney et al. 2014) and give us the ability to compute the emergent spectra, we will be in a position to make quantitative predictions for spectra and variability of accreting BHs. This will allow us to carry out precision experiments that will test theoretical models of BH accretion and jets on a new quantitative level and give us the ability to measure masses and spins for a large number of BHs.

---

[6]With radiation feedback on the structure of the accretion flow accounted for, the ratio $\dot{M}/\dot{M}_{\mathrm{Edd}}$ is expected to determine the accretion disk angular thickness, h/r, which controls the strength of BH magnetic flux and jet power in the MAD state.

References

Allen, S.W., Dunn, R.J.H., Fabian, A.C., Taylor, G.B., Reynolds, C.S.: MNRAS **372**, 21 (2006)

Balbus, S.A., Hawley, J.F.: ApJ **376**, 214 (1991)

Bardeen, J.M.: Nature **226**, 64 (1970)

Barkov, M.V., Baushev, A.N.: New Astron. **16**, 46 (2011)

Beckwith, K., Hawley, J.F., Krolik, J.H.: ApJ **678**, 1180 (2008)

Begelman, M.C.: Accretion disks in active galactic nuclei. In: Miller, J.S. (ed.) Astrophysics of Active Galaxies and Quasi-Stellar Objects, pp. 411–452. University Science Books, Mill Valley (1985)

Begelman, M.C., Armitage, P.J.: ApJ **782**, L18 (2014)

Berger, E., Zauderer, A., Pooley, G.G., et al.: ApJ **748**, 36 (2012)

Bisnovatyi-Kogan, G.S., Ruzmaikin, A.A.: Ap&SS **28**, 45 (1974)

Bisnovatyi-Kogan, G.S., Ruzmaikin, A.A.: Ap&SS **42**, 401 (1976)

Blandford, R.D.: Beyond the fringe. In: Romney, J., Reid, M. (eds.) Future Directions in High Resolution Astronomy. Astronomical Society of the Pacific Conference Series, vol. 340, p. 3. Astronomical Society of the Pacific, San Francisco (2005)

Blandford, R.D., Payne, D.G.: MNRAS **199**, 883 (1982)

Blandford, R.D., Znajek, R.L.: MNRAS **179**, 433 (1977)

Bloom, J.S., et al.: Science **333**, 203 (2011)

Burrows, D.N., et al.: Nature **476**, 421 (2011)

Cenko, S.B., et al.: ApJ **753**, 77 (2012)

Chakrabarti, S.K.: ApJ **288**, 1 (1985)

Chiueh, T., Li, Z.Y., Begelman, M.C.: ApJ **377**, 462 (1991)

Cowperthwaite, P.S., Reynolds, C.S.: ApJ **752**, L21 (2012)

Davis, S.W., Narayan, R., Zhu, Y., Barret, D., Farrell, S.A., Godet, O., Servillat, M., Webb, N.A., ApJ **734**, 111 (2011)

De Villiers, J.P., Hawley, J.F.: ApJ **589**, 458 (2003)

De Villiers, J.P., Hawley, J.F., Krolik, J.H.: ApJ **599**, 1238 (2003)

De Villiers, J.P., Hawley, J.F., Krolik, J.H., Hirose, S.: ApJ **620**, 878 (2005)

Dexter, J., McKinney, J.C., Markoff, S., Tchekhovskoy, A.: MNRAS **440**, 2185 (2014)

Eatough, R.P., Falcke, H., Karuppusamy, R., Lee, K.J., Champion, D.J., Keane, E.F., Desvignes, G., Schnitzeler, D.H.F.M., Spitler, L.G., Kramer, M., Klein, B., Bassa, C., Bower, G.C., Brunthaler, A., Cognard, I., Deller, A.T., Demorest, P.B., Freire, P.C.C., Kraus, A., Lyne, A.G., Noutsos, A., Stappers, B., Wex, N.: Nature **501**, 391 (2013)

Esin, A.A., McClintock, J.E., Narayan, R.: ApJ **489**, 865 (1997)

Esin, A.A., Narayan, R., Cui, W., Grove, J.E., Zhang, S.N.: ApJ **505**, 854 (1998)

Fabian, A., Iwasawa, K., Reynolds, C., Young, A.: Publ. Astron. Soc. Pac. **112**(775), 1145 (2000)

Fanaroff, B.L., Riley, J.M.: MNRAS **167**, 31P (1974)

Farrell, S.A., Webb, N.A., Barret, D., Godet, O., Rodrigues, J.M.: Nature **460**(7251), 73 (2009)

Fender, R.P., Belloni, T.M., Gallo, E.: MNRAS **355**, 1105 (2004)

Fender, R.P., Gallo, E., Russell, D.: MNRAS **406**, 1425. ArXiv:1003.5516 (2010)

Fernandes, C.A.C. et al.: MNRAS **411**, 1909 (2011)

Fragile, P.C., Blaes, O.M., Anninos, P., Salmonson, J.D.: ApJ **668**, 417 (2007)

Frank, J., King, A., Raine, D.J.: Accretion Power in Astrophysics, 3rd edn. Cambridge University Press, Cambridge (2002)

Gammie, C.F., Narayan, R., Blandford, R.: ApJ **516**, 177 (1999)

Gammie, C.F., McKinney, J.C., Tóth, G.: ApJ **589**, 444 (2003)

Gammie, C.F., Shapiro, S.L., McKinney, J.C.: ApJ **602**, 312 (2004)

Ghisellini, G., et al.: MNRAS **402**, 497 (2010)

Ghosh, P., Abramowicz, M.A.: MNRAS **292**, 887 (1997)

Giannios, D., Metzger, B.D.: MNRAS **416**, 2102 (2011)

Guilet, J., Ogilvie, G.I.: MNRAS **424**, 2097 (2012)

Guilet, J., Ogilvie, G.I.: MNRAS **430**, 822 (2013)
Hawley, J.F., Krolik, J.H.: ApJ **641**, 103 (2006)
Heinz, S., Sunyaev, R.A.: MNRAS **343**, L59 (2003)
Hui, Y., Krolik, J.H.: ApJ **679**, 1405 (2008)
Igumenshchev, I.V.: ApJ **677**, 317 (2008)
Igumenshchev, I.V.: ApJ **702**, L72 (2009)
Igumenshchev, I., Narayan, R., Abramowicz, M.: ApJ **592**, 1042 (2003)
Komissarov, S.S.: MNRAS **326**, L41 (2001)
Komissarov, S.S., Barkov, M.V.: MNRAS **397**, 1153 (2009)
Krolik, J.H., Hawley, J.F., Hirose, S.: ApJ **622**, 1008 (2005)
Kulkarni, A.K., Penna, R.F., Shcherbakov, R.V., Steiner, J.F., Narayan, R., Sä Dowski, A., Zhu,
    Y., McClintock, J.E., Davis, S.W., McKinney, J.C.: MNRAS **414**, 1183 (2011)
Livio, M., Ogilvie, G.I., Pringle, J.E.: ApJ **512**, 100 (1999). doi:10.1086/306777
Lubow, S.H., Papaloizou, J.C.B., Pringle, J.E.: MNRAS **267**, 235 (1994)
Maccarone, T.J.: A&A **409**, 697 (2003)
MacFadyen, A.I., Woosley, S.E.: ApJ **524**, 262 (1999)
Martínez-Sansigre, A., Rawlings, S.: MNRAS **414**, 1937 (2011)
McClintock, J.E., Narayan, R., Davis, S.W., Gou, L., Kulkarni, A., Orosz, J.A., Penna, R.F.,
    Remillard, R.A., Steiner, J.F.: Class. Quantum Gravity **28**(11), 114009 (2011)
McClintock, J.E., Narayan, R., Steiner, J.F.: Space Sci. Rev., **183**, 295–322 (2013)
McKinney, J.C.: ApJ **630**, L5 (2005)
McKinney, J.C., Blandford, R.D.: MNRAS **394**, L126 (2009)
McKinney, J.C., Gammie, C.F.: ApJ **611**, 977 (2004)
McKinney, J.C., Tchekhovskoy, A., Blandford, R.D.: MNRAS **423**, 3083 (2012)
McKinney, J.C., Tchekhovskoy, A., Blandford, R.D.: Science **339**, 49 (2013)
McKinney, J.C., Tchekhovskoy, A., Sadowski, A., Narayan, R.: MNRAS **441**, 3177 (2014)
McNamara, B.R., Kazemzadeh, F., Rafferty, D.A., Bîrzan, L., Nulsen, P.E.J., Kirkpatrick,
    C.C., Wise, M.W.: ApJ **698**, 594 (2009)
McNamara, B.R., Rohanizadegan, M., Nulsen, P.E.J.: ApJ **727**, 39 (2011)
Metzger, B.D., Giannios, D., Mimica, P.: MNRAS **420**, 3528 (2012)
Narayan, R., McClintock, J.E.: MNRAS **419**, L69 (2012)
Narayan, R., Igumenshchev, I.V., Abramowicz, M.A.: PASJ **55**, L69 (2003)
Narayan, R., Sądowski, A., Penna, R.F., Kulkarni, A.K.: MNRAS **426**, 3241 (2012)
Nemmen, R.S., Tchekhovskoy, A.: MNRAS (2014, submitted). ArXiv:1406.7420
Novikov, I.D., Thorne, K.S.: Astrophysics of black holes. In: De Witt, C., De Witt, B.S. (eds.)
    Black Holes-Les Astres Occlus. Gordon & Breach, New York (1973)
Penna, R.F., et al.: MNRAS **408**, 752 (2010)
Popham, R., Woosley, S.E., Fryer, C.: ApJ **518**, 356 (1999)
Potter, W.J., Balbus, S.A.: MNRAS **441**, 681 (2014)
Proga, D., Begelman, M.C.: ApJ **592**, 767 (2003)
Punsly, B.: ApJ **728**, L17 (2011)
Rawlings, S., Saunders, R.: Nature **349**, 138 (1991)
Rees, M.J.: Nature **333**, 523 (1988)
Remillard, R.A., McClintock, J.E.: ARA&A **44**, 49 (2006)
Reynolds, C.S.: Space Sci. Rev., **183**, 277–294 (2013a)
Reynolds, C.S.: Class. Quantum Gravity **30**(24), 244004 (2013b)
Rothstein, D.M., Lovelace, R.V.E.: ApJ **677**, 1221 (2008)
Russell, D.M., Miller-Jones, J.C.A., Maccarone, T.J., Yang, Y.J., Fender, R.P., Lewis, F.: ApJ **739**,
    L19 (2011)
Russell, D.M., Gallo, E., Fender, R.P.: MNRAS **431**, 405 (2013)
Sądowski, A., Narayan, R., Penna, R., Zhu, Y.: MNRAS **436**, 3856 (2013)
Sądowski, A., Narayan, R., McKinney, J.C., Tchekhovskoy, A.: MNRAS **439**, 503 (2014)
Shafee, R., McKinney, J.C., Narayan, R., Tchekhovskoy, A., et al.: ApJ **687**, L25 (2008)
Shakura, N.I., Sunyaev, R.A.: A&A **24**, 337 (1973)

Shapiro, S.L., Teukolsky, S.A. (eds.): Black Holes, White Dwarfs and Neutron Stars: The Physics of Compact Objects, pp. 672. Wiley-VCH, Weinheim (1986). ISBN:0-471-87316-0

Sikora, M., Stawarz, Ł., Lasota, J.P.: ApJ **658**, 815 (2007)

Steiner, J.F., McClintock, J.E., Narayan, R.: ApJ **762**, 104 (2013)

Stone, N., Loeb, A.: PRL **108**(6), 061302 (2012)

Straub, O., Godet, O., Webb, N., Servillat, M., Barret, D.: ArXiv e-prints (2014)

Tanabe, K., Nagataki, S.: Phys. Rev. D **78**(2), 024004 (2008)

Tavecchio, F., Becerra-Gonzalez, J., Ghisellini, G., Stamerra, A., Bonnoli, G., Foschini, L., Maraschi, L.: A&A **534**, A86 (2011)

Tchekhovskoy, A., Giannios, D.: MNRAS (2014, submitted). ArXiv:1409.4414

Tchekhovskoy, A., McKinney, J.C.: MNRAS **423**, L55 (2012)

Tchekhovskoy, A., McKinney, J.C., Narayan, R.: MNRAS **379**, 469 (2007)

Tchekhovskoy, A., McKinney, J.C., Narayan, R.: MNRAS **388**, 551 (2008)

Tchekhovskoy, A., McKinney, J.C., Narayan, R.: ApJ **699**, 1789 (2009)

Tchekhovskoy, A., Narayan, R., McKinney, J.C.: ApJ **711**, 50 (2010)

Tchekhovskoy, A., Narayan, R., McKinney, J.C.: New Astron. **15**, 749 (2010)

Tchekhovskoy, A., Narayan, R., McKinney, J.C.: MNRAS **418**, L79 (2011)

Tchekhovskoy, A., McKinney, J.C., Narayan, R.: J. Phys. Conf. Ser. **372**(1), 012040 (2012)

Tchekhovskoy, A., Metzger, B.D., Giannios, D., Kelley, L.Z.: MNRAS **437**, 2744 (2014)

Thorne, K.S.: ApJ **191**, 507 (1974)

Ulmer, A.: ApJ **514**, 180 (1999)

Urry, C.M., Padovani, P.: PASP **107**, 803 (1995)

van Velzen, S., Falcke, H.: A&A **557**, L7 (2013)

Webb, N., Cseh, D., Lenc, E., Godet, O., Barret, D., Corbel, S., Farrell, S., Fender, R., Gehrels, N., Heywood, I.: Science **337**, 554 (2012)

Wiersema, K., van der Horst, A.J., Levan, A.J., et al.: MNRAS **421**, 1942 (2012)

Woosley, S.E.: ApJ **405**, 273 (1993)

Yuan, F., Narayan, R.: ARA&A, **52**, 529. ArXiv e-prints (2014)

Yuan, F., Quataert, E., Narayan, R.: ApJ **598**, 301 (2003)

Zamaninasab, M., Clausen-Brown, E., Savolainen, T., Tchekhovskoy, A.: Nature **510**(7503), 126 (2014)

Zauderer, B.A., Berger, E., Soderberg, A.M., et al.: Nature **476**, 425 (2011)

Zauderer, B.A., Berger, E., Margutti, R., Others.: ApJ **767**, 152 (2013)

Zhu, Y., Davis, S.W., Narayan, R., Kulkarni, A.K., Penna, R.F., McClintock J.E.: MNRAS **424**, 2504 (2012)